ANALYSING AND COMPUTING
TURBULENT FLOWS
USING WAVELETS

MARIE FARGE   KAI SCHNEIDER

LMD-CNRS,   *CMI,*
Ecole Normale Supérieure,   *Université de Provence,*
24 rue Lhomond,   *39 rue Joliot–Curie,*
75231 Paris Cedex 05, France *13453 Marseille Cedex 13, France*

Contents

IV   Conclusion   52

ANALYSING AND COMPUTING
TURBULENT FLOWS
USING WAVELETS

Marie Farge[1] & Kai Schneider[2]

Abstract

These lecture notes are a review on wavelet techniques for ana-
lyzing and computing fully-developed turbulent flows, which corre-
spond to the regime where nonlinear instabilities are dominant. The
wavelet-based techniques we have been developing during the last
decade are explained and the main results are presented. After in-
troducing the continuous and discrete wavelet transforms we present
classical and wavelet-based statistical diagnostics to study turbulent
flows. We then present wavelet methods for extracting coherent vor-
tices in two- and three-dimensional turbulent flows. Afterwards we
present an adaptive wavelet solver for the two-dimensional Navier–
Stokes equations and apply it to compute a time-developing turbulent
mixing layer. Finally we draw some conclusions and present some
perspectives for turbulence modelling.

1   Introduction

This chapter will focus on fully-developed turbulence in incompressible
flows. By fully-developed turbulence we mean the limit for which the non-
linear advective term of Navier-Stokes equations is larger by several orders
of magnitude than the linear dissipative term. The ratio between both
terms is defined as the Reynolds number Re, which is related to the ratio
of the large excited scales and the small scales where dissipation damps
any instabilities. In practically relevant applications (*e.g.* aeronautics, me-
teorology, combustion...) Re varies in between 10^6 and 10^{12}. For Direct
Numerical Simulation (DNS), where all scales are resolved, the number of

---

[1] LMD-CNRS, Ecole Normale Supérieure, Paris, France
[2] CMI, Université de Provence, Marseille, France

degrees of freedom to be computed scales as Re for two-dimensional flows and as $Re^{9/4}$ for three-dimensional flows. Consequently one cannot integrate Navier–Stokes equations in the fully-developed turbulence regime with present computers without using some *ad hoc* turbulence model. Its role consists in reducing the dimension of the system of equations to be computed. Typically the degrees of freedom are split into two subsets: the active modes to be computed and the passive modes to be modelled. The number of active modes should be as small as possible while the number of passive modes should be as large as possible.

A classical approach to compute fully-developed turbulent flows is Large Eddy Simulation (LES) [37] where the separation is done by means of linear filtering between large-scale modes, assumed to be active, and small-scale modes, assumed to be passive. This means that the flow evolution is calculated deterministically up to the cutoff scale, whereas the influence of the subgrid scales onto the resolved scales is statistically modelled, *e.g.* using Smagorinsky's parametrization. As consequence vortices in strong nonlinear interaction are smoothed and instabilities which may develop at subgrid scales are ignored. Indeed LES models have problems to deal with backscatter, *i.e.* transfers from subgrid scales towards resolved scales due to nonlinear instabilities. The dynamical LES model [32] takes into account backscatter, but only in a locally averaged way. A further step in the hierarchy of turbulence models are the Reynolds Averaged Navier–Stokes (RANS) equations where the time-averaged mean flow is computed while fluctuations are modelled, in which case only steady state solutions are predicted. This leads to turbulence models such as k-ϵ or Reynolds stress models, extensively used in industry. It should be stressed that such low-order turbulence models are lacking universality, in the sense that one should adjust the parameters of the model from laboratory measurements for each flow configuration, and sometimes different parameters are even needed for different regions of the flow.

Turbulent flows are characterized by their unpredictability, namely each flow realization is different although the statistics are reproducible as long as the flow configuration and parameters are the same. One observes in each flow realization the formation of localized coherent vortices whose motions are chaotic, resulting from their mutual interactions. The statistical theory of homogeneous and isotropic turbulence [2, 35, 36, 43] is based on L^2-norm ensemble averages and therefore is unsensitive to the presence of coherent vortices which contribute too weakly to the L^2-norm. In opposition to this approach one can consider that coherent vortices are the fundamental components of turbulent flows [49] and therefore both numerical and statistical models should take them into account. In the present lecture notes we

propose a new semi-deterministic approach which reconciles both, the statistical and the deterministic points of view. This technique is based on the space and scale decomposition of the flow using the wavelet representation.

Wavelet methods have been introduced during the last decade to analyze, model and compute fully-developed turbulent flows [6,14,17,28,29,51]. For recent overview of wavelets and turbulence, we refer the reader to [20,22,53]. The main result is that the wavelet representation is able to disentangle coherent vortices from incoherent background flow in two-dimensional turbulent flows. Both components are multiscale but present different statistics with different correlations. The coherent vortex components present non-Gaussian distribution and long-range correlation, while the incoherent background flow components are characterized by Gaussian statistics and short-range correlation [16,19,21]. This leads to propose a new way to split turbulent dynamics into: active coherent vortex modes, to be computed in a wavelet basis dynamically adapted to follow their motion, and passive incoherent modes, to be statistically modelled as a Gaussian random process. This new approach, called Coherent Vortex Simulation (CVS) [21], differs significantly from LES. LES is based on linear filtering (defined either in physical space or in Fourier space) between large and small scales, but without a clearcut separation between Gaussian and non-Gaussian behaviours. CVS uses nonlinear filtering (defined in wavelet space) between Gaussian and non-Gaussian modes having different scaling laws, but without any clearcut scale separation. The advantage of CVS method compared to LES is to reduce the number of computed active modes for a given Reynolds number [16] and to control the Gaussianity of the passive degrees of freedom to be statistically modelled [21].

These lecture notes are organized in three parts: wavelet transforms, turbulence analysis and turbulence computation. In the first part we present both the continuous and the orthogonal wavelet transforms in one and several dimensions, together with the corresponding algorithms. In the second part, after a brief review of classical statistical tools for analysing turbulence, we present wavelet-based statistical tools, such as local and global wavelet spectra and discuss their relation with the Fourier spectrum. We also introduced several wavelet-based measures to characterize and quantify the intermittency, property which is generic for turbulence. In the last part, we present a new approach, called Coherent Vortex Simulation (CVS), which computes turbulent flows for regimes where their dynamics is dominated by coherent vortices. We first show how to extract coherent vortices out of turbulent flows, and we illustrate this method for a 3D turbulent mixing layer. Then, after a brief review of classical methods for computing turbulent flows, we expose the principle of CVS. Finally we describe the algorithm for computing 2D Navier-Stokes equations in an adaptive wavelet

basis and we apply it to simulate a 2D turbulent mixing layer.

Part I
Wavelet Transforms

2 History

Wavelets have been developed in the beginning of eighties in France [31]. This recent mathematical technique is based on group theory and square integrable representations, which allows the decomposition of a signal, or a field, into both space and scale, and possibly directions [14]. To motivate the use of wavelets in relation with turbulence, we briefly recall some fundamental ideas and mention several fields of applications. For details we refer the reader to textbooks [8, 39, 42]. From an abstract point of view wavelets constitute new 'atoms' and 'molecules', *i.e.* basic building blocks of various function spaces out of which some can be used to contruct orthogonal bases. The starting point is a function $\psi(x)$, called mother wavelet. This function is assumed to be well-localized, i.e. ψ exhibits a fast decay for $|x|$ tending to infinity, is oscillating, *i.e.* ψ has at least a vanishing integral (the mean value is zero) or better the first m moments of ψ vanish, and is smooth, i.e. $\hat{\psi}$ the Fourier transform of ψ exhibits fast decay in wavenumber space $|k|$.

The mother wavelet then generates a family of wavelets $\psi_{l,x}(x')$ by dilatation (or contraction) by the parameter $l > 0$ and translation by the parameter $x \in \mathbb{R}$, i.e. $\psi_{l,x}(x') = l^{-1/2}\psi(\frac{x'-x}{l})$, where all wavelets being normalized in L^2-norm. An example of such a family (for discrete l and x) is depicted in Fig.1. The wavelet transform of a function f is then defined as a convolution of the analysing wavelet with the signal f, $\tilde{f}(l,x) = \int f(x')\psi_{l,x}(x')dx'$. The wavelet coefficients $\tilde{f}(l,x)$ measure the fluctuations of f around the point x and scale (frequency) l. The function f can be reconstructed as a linear combination of wavelets $\psi_{l,x}(x')$ with coefficients $\tilde{f}(l,x)$ [31], e.g. $f(x) = 1/C_\psi \int \int \tilde{f}(l,x)\psi_{l,x}(x')l^{-2}\,dldx$, C_ψ being a constant which depends on the wavelet ψ. Let us mention that due to the localization of wavelets in physical space the behaviour of the signal at infinity does not play any role. Therefore the wavelet analysis and synthesis can be performed locally as opposed to the Fourier transform where a global behaviour is intrinsically implicated through the nonlocal nature of the trigonometric functions.

The origin of wavelets is interdisciplinary. Wavelets come from different fields such as engineering (subband coding, quadrature mirror filters, time–frequency analysis), theoretical physics (coherent states of affine groups in quantum mechanics) and mathematics (Calderon–Zygmund operators,
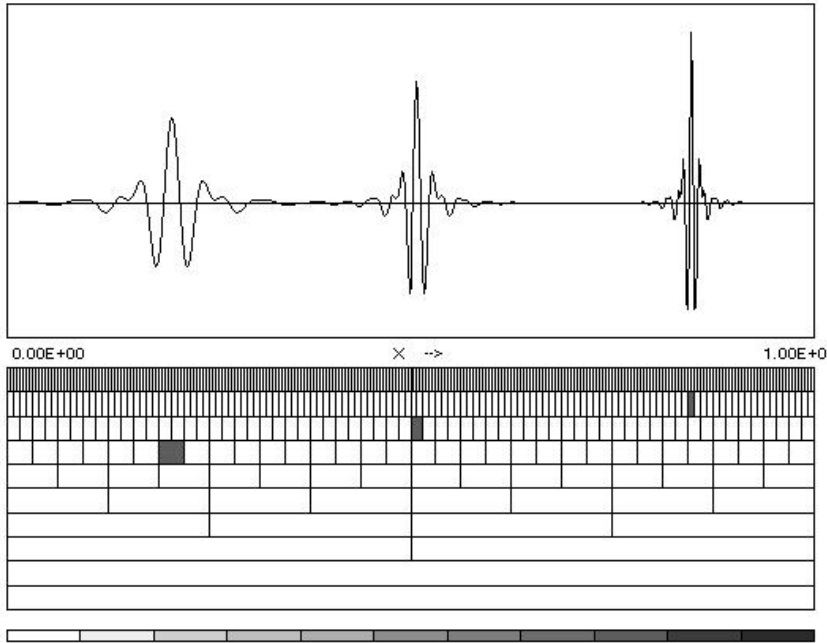
Fig. 1. Example: Discrete wavelets $\psi_{j,k}(x) = l_0^{j/2}\,\psi(l_0^j x' - kx_0)$ with $l_0 = 2$ and $x_0 = 1$ and $l = l_0^j$, $x = kx_0 l_0^j$ for the case of orthogonal quintic spline wavelets $\psi_{5,6}(x')$, $\psi_{6,32}(x')\ \psi_{7,108}(x')$.

characterization of function spaces). Meanwhile a large spectrum of applications has grown and is still developing, ranging from signal or image analysis and processing, to numerical analysis.

3   The continuous wavelet transform

3.1   One dimension

3.1.1   Analyzing wavelet

Starting point for the wavelet transform is a real or complex valued function $\psi(x)$, called wavelet, which has to fulfill the admissibility condition,

$$C_\psi = \int_0^\infty \left|\widehat{\psi}(k)\right|^2 \frac{dk}{|k|} \ < \ \infty \qquad\qquad (3.1)$$

where

$$\widehat{\psi}(k) = \frac{1}{2\pi}\int_{-\infty}^\infty \psi(x)e^{-i2\pi kx}\,dx \qquad\qquad (3.2)$$

denotes the Fourier transform. If ψ is integrable this implies that ψ has zero mean,

$$\int_{-\infty}^{\infty} \psi(x)dx \;=\; 0 \qquad \text{or} \quad \widehat{\psi}(k=0) \;=\; 0. \tag{3.3}$$

In practice however one also requires that the wavelet ψ should be well–localized in both physical and Fourier spaces, which implies smoothness. We also require that higher order moments of ψ vanish, $i.e.$

$$\int_{-\infty}^{\infty} x^m \psi(x)dx \;=\; 0 \qquad \text{for} \quad m = 0, M \tag{3.4}$$

which means that monomials up to degree M are exactly reproduced. In Fourier space this property is equivalent to

$$\frac{d^m}{dk^n} \, \widehat{\psi}(k)|_{k=0} \;=\; 0 \qquad \text{for} \quad m = 0, M \tag{3.5}$$

so that the Fourier transform of ψ decays smoothly at $k = 0$.

3.1.2   Wavelet analysis

From this function ψ, the so–called mother wavelet, we generate a family of continuously translated and dilated wavelets, normalized in L^2–norm

$$\psi_{l,x}(x') = l^{-1/2} \, \psi(\frac{x'-x}{l}) \qquad \text{for} \quad l > 0 \qquad \text{and} \quad x \in I\!\!R \tag{3.6}$$

where l denotes the scale dilation parameter, corresponding to the width of the wavelet and x the translation parameter, corresponding to the position of the wavelet.
In Fourier space this reads

$$\widehat{\psi}_{l,x}(k) = \sqrt{l} \, \widehat{\psi}(lk) \, e^{-i2\pi kx} \tag{3.7}$$

where the contraction with $1/l$ is reflected in a dilation with l and the translation with x implies a rotation in the complex plane.

The continuous wavelet transform of a signal f is then defined as a convolution of f with the wavelet family $\psi_{l,x}$

$$\tilde{f}(l,x) = \int_{-\infty}^{\infty} f(x')\overline{\psi}_{l,x}(x')dx' \tag{3.8}$$

where $\overline{\psi}_{l,x}$ denotes in the case of complex valued wavelets the complex conjugate.
Using Parseval's identity we also get

$$\tilde{f}(l,x) = \int_{-\infty}^{\infty} \hat{f}(k)\overline{\widehat{\psi}_{l,x}}(k)dk \tag{3.9}$$

so that the wavelet transform may be interpreted as a frequency decomposition using band pass filters $\hat{\psi}_{l,x}$ centered at frequency $k = \frac{k_0}{l}$, where k_0 denotes the center of the wavelet in Fourier space, and having variable width $\frac{Deltak}{k}$, so for increasing scales the bandwidth is getting wider.

3.1.3   Wavelet synthesis

The admissibility condition (3.1) of ψ implies the existence of a finite energy reproducing kernel, see *e.g.* [8], which is a necessary condition for being able to reconstruct a function from its wavelet coefficients. The signal can thus be reconstructed entirely from its wavelet coefficients,

$$f(x) = \frac{1}{C_\psi} \int_0^\infty \int_{-\infty}^\infty \tilde{f}(l, x)\, \psi_{l,x}(x')\, \frac{dl\, dx}{l^2} \tag{3.10}$$

which is the inverse wavelet transform.

3.1.4   Energy conservation

There also holds an energy conservation like for Fourier transforms, *i.e.* a Plancherel identity, which means that the total energy of a signal can be either calculated in physical space or in wavelet coefficient space,

$$\int_{-\infty}^\infty |f(x)|^2\, dx \;=\; \frac{1}{C_\psi} \int_0^\infty \int_{-\infty}^\infty |\tilde{f}(l, x)|^2\, \frac{dl\, dx}{l^2} \tag{3.11}$$

This formula is also the starting point for the definition of wavelet spectra.

3.2   Higher dimensions

The theory of the continuous wavelet transform can be generalized in several dimensions [44] using rotation in addition to dilatation and translation. For a two-dimensional function $f \in L^2(\mathbb{R}^2)$ (constructions for higher dimensions are analogous) we get

$$\tilde{f}(l, \vec{x}, \theta) \;=\; \int\!\!\int_{\mathbb{R}^2} f(\vec{x}')\, \overline{\psi}_{l,\vec{x},\theta}(\vec{x}')\, d^2\vec{x}' \quad \text{for} \quad l > 0,\; \theta \in [0, 2\pi[,\; \vec{x} \in \mathbb{R}^2 \tag{3.12}$$

where the family of functions $\psi_{l,\vec{x},\theta}$ is obtained from a single one ψ by dilatation with l^{-1}, by translation by $\vec{x}$ and by rotation of angle θ,

$$\psi_{l,\vec{x},\theta}(\vec{x}') \;=\; \frac{1}{l}\psi(R_\theta(\frac{\vec{x}' - \vec{x}}{l})) \tag{3.13}$$

where R_θ denotes a rotation matrix.
Analoguously to the one-dimensional case this transformation is invertible

and isometric, provided that ψ fulfills the admissibility condition

$$C_\psi = \int \int_{I\!\!R^2} \left| \widehat{\psi}(\vec{k}) \right|^2 \frac{d^2 \vec{k}}{|\vec{k}|^2} \; < \; \infty \qquad (3.14)$$

In the following we restrict ourselves to isotropic real-valued wavelets, so there is no more a dependence on θ. The wavelet coefficients can then be calculated using the formula

$$\tilde{f}(l,\vec{x}) \; = \; \int \int_{I\!\!R^2} \; \widehat{f}(\vec{k}) \, l \overline{\widehat{\psi}}(l\vec{k}) \, e^{i 2\pi \vec{k}\cdot\vec{x}} \; d^2\vec{k} \qquad (3.15)$$

where the Fourier transform of the wavelet ψ_l is essentially supported on an annulus a radius l^{-1}.
The energy conservation reads

$$\int \int_{I\!\!R^2} |f(\vec{x})|^2 \, d\vec{x} \; = \; \frac{1}{C_\psi} \int_0^\infty \int \int_{I\!\!R^2} \; |\tilde{f}(l,\vec{x})|^2 \, \frac{dl \, d^2 \vec{x}}{l^3} \qquad (3.16)$$

and the function f can be reconstructed entirely from its wavelet coefficients by the relation

$$f(\vec{x}') = \frac{1}{C_\psi} \; \int_0^\infty \int \int_{I\!\!R^2} \; \tilde{f}(l,\vec{x}) \, \psi_l(\vec{x}' - \vec{x}) \frac{d^2 \vec{x} \, dl}{l^3}. \qquad (3.17)$$

3.3   Algorithm

To illustrate the practical implementation of the continuous wavelet transform we consider a one-dimensional signal $f(x)$ sampled on a regular grid with $N = 2^J$ points, *i.e.* $f(i/2^J)$ for $i = 0,...,2^J - 1$ are given. We assume the signal to be periodic and compute the wavelet coefficients by means of the Fast Fourier Transform (FFT). The large scale corresponds to the domaine size which is by construction equal to 1. The smaller scales are discretized logarithmically,

$$l_j \; = \; l_0^{-j} \qquad j \geq 0 \quad . \qquad (3.18)$$

The choise of l_0 is determined by the reconstruction formula to ensure a given precision for the reconstruction of the signal by a discretized version of formula (3.10). For wavelets being derivatives of Gaussians the choice of $l_0 = 2^{1/4}$ is sufficiently precise as discussed in [8]. The smallest scale of the discretization corresponds to $\frac{2}{N} = 2^{1-J}$.

To compute $\tilde{f}(l,x)$ we discretize the formula (3.9). First we compute the disrete Fourier transform of the signal samples. Then we multiply it with the wavelet filter in Fourier space and we obtain subsequently at each scale

l_j for $j = 0$ to $J - 1$ simultaneously at all positions $x_n = \frac{n}{N}, n = 0, N - 1$ the wavelet coefficients by executing an inverse FFT

$$\tilde{f}(l_j, x_n) = \sum_{k=-N/2}^{N/2-1} \widehat{f}_k \sqrt{l_j} \, \overline{\psi(\widehat{l_j k})} e^{+i2\pi kn/N} \qquad (3.19)$$

where $\widehat{f}_k$ denotes the discrete Fourier transform of the samples $f\left(\frac{n}{N}\right)$,

$$\widehat{f}_k = \frac{1}{N} \sum_{n=0}^{N-1} f\left(\frac{n}{N}\right) e^{-i2\pi nk/N} \qquad (3.20)$$

Due to periodicity of the signal f no boundary effects are introduced by using the FFT. The complexity of the algorithm is of order $N \log N$ at each scale due to the use of the FFT.

The above algorithm can be applied analoguously in the two-dimensional case using tensor product discretization together with 2D FFTs.

4   The orthogonal wavelet transform

4.1   One dimension

In this section we recall some essential features of the discrete wavelet approximation on the real line, *i.e.* in $L^2(\mathbb{R})$ that will be important in the sequel. For an exhaustive treatment we refer the reader to [8, 39, 42].

4.1.1   1D Multi-Resolution Analysis

The discrete wavelet transform relies on the concept of Multi-Resolution Analysis (MRA) which is a sequence of imbedded subspaces V_j verifying

$$V_j \subset V_{j+1} \qquad \forall j \in \mathbb{Z} \qquad (4.1)$$

$$\overline{\bigcup}_{j \in \mathbb{Z}} V_j = L^2(\mathbb{R}) \qquad (4.2)$$

$$\bigcap_{j \in \mathbb{Z}} V_j = \{0\} \qquad (4.3)$$

$$f(x) \in V_j \Leftrightarrow f(2x) \in V_{j+1} \qquad (4.4)$$

A scaling function $\phi(x)$ is required to exist. Their translates generate a basis in each V_j, *i.e.*

$$V_j = \overline{span}\{\phi_{ji}\}_{i \in \mathbb{Z}} \quad . \qquad (4.5)$$

where

$$\phi_{ji}(x) = 2^{j/2}\phi(2^j x - i) \qquad\qquad j, i \in \mathbb{Z} \quad . \tag{4.6}$$

In the classical case this basis is orthonormal, so that

$$< \phi_{ji}, \phi_{jk} >_{\mathbb{R}} = \delta_{ik} \tag{4.7}$$

with $< f, g >_{\mathbb{R}} = \int_{-\infty}^{+\infty} f(x)\,\overline{g}(x)\,dx$ being the inner product in $L^2(\mathbb{R})$.

The main issue of the wavelet approach now is to work with the orthogonal complement spaces W_j defined by

$$V_{j+1} = V_j \oplus W_j \tag{4.8}$$

Based on the function $\phi(x)$ one can find a function $\psi(x)$, the so-called mother wavelet. Their translates and dilates constitute a orthonormal bases of the spaces W_j,

$$W_j = \overline{span}\{\psi_{ji}\}_{i \in \mathbb{Z}} \tag{4.9}$$

where

$$\psi_{ji}(x) = 2^{j/2}\psi(2^j x - i) \qquad\qquad j, i \in \mathbb{Z} \tag{4.10}$$

Each function $f \in L^2(\mathbb{R})$ can now be expressed as

$$f(x) = \sum_{i \in \mathbb{Z}} \overline{f}_{j_0 i}\, \phi_{j_0 i}(x) \quad + \quad \sum_{j=j_0}^{\infty} \sum_{i \in \mathbb{Z}} \tilde{f}_{ji}\, \psi_{ji}(x) \tag{4.11}$$

where

$$\overline{f}_{ji} = < f, \phi_{ji} >_{\mathbb{R}} \qquad \tilde{f}_{ji} = < f, \psi_{ji} >_{\mathbb{R}} \tag{4.12}$$

In numerical applications the sums in (4.11) have to be truncated which corresponds to the projection of f onto a subspace of $V_J \subset L^2(\mathbb{R})$. The decomposition (4.11) is orthogonal, as, by construction,

$$< \psi_{ji}, \psi_{lk} >_{\mathbb{R}} \;=\; \delta_{jl}\,\delta_{ik} \tag{4.13}$$

$$< \psi_{ji}, \phi_{lk} >_{\mathbb{R}} \;=\; 0 \qquad\qquad j \geq l \tag{4.14}$$

in addition to (4.7).

4.1.2   Regularity and local decay of wavelet coefficients

The relation between the local or global regularity of a function and the decay of its wavelet coefficients is well known. The global regularity directly determines the error being made when the wavelet sum is truncated at some scale. Depending on the type of norm and whether global or local characterization is concerned, various relations of this kind have been

developed, see *e.g.* [8, 39, 42] for an overview. As an example we consider the case of an α-Lipschitz function, with $\alpha \geq 1$ [33]. Suppose $f \in L^2(\mathbb{R})$, then for $[a, b] \subset \mathbb{R}$ the function f is α-Lipschitz for any $x_0 \in [a, b]$, *i.e.* $|f(x_0 + h) - f(x_0)| \leq C|h|^\alpha$, if and only if there exists a constant A such that $| <f, \psi_{ji}> | \leq A 2^{-j\alpha - \frac{1}{2}}$ for any (j, i) with $\frac{i}{2^j} \in]a, b[$. This shows the relation between the local regularity of a function and the decay of its wavelet coefficients in scale. The adaptive discretization discussed in the present lecture notes is precisely based on taking into account spatially varying regularity of the solution through a variable cut off in scale of its wavelet series.

4.2   Higher dimensions

This section consists of an extension of the previously presented one-dimensional construction to higher dimensions. For simplicity, we will consider only the two-dimensional case, since higher dimensions can be treated analogously [8, 39, 42]. We start with a brief description of the construction principle and then turn in more detail to the two-dimensional case with periodicity, which is relevant for the subsequent applications.

4.2.1   Tensor product construction

Having developed a one-dimensional orthonormal basis ψ_{ji} of $L^2(\mathbb{R})$ one would like to use these functions as building blocks in higher dimensions. One way of doing so is to take the tensor product of two one-dimensional bases [8] and to define

$$\psi_{j_x, j_y, i_x, i_y}(x, y) \;=\; \psi_{j_x, i_x}(x)\, \psi_{j_y, i_y}(y) \qquad (4.15)$$

The resulting functions constitute an orthonormal wavelet basis of $L^2(\mathbb{R}^2)$. Each function $f \in L^2(\mathbb{R}^2)$ can then be developed into

$$f(x, y) \;=\; \sum_{j_x, i_x} \sum_{j_y, i_y} d_{j_x, j_y, i_x, i_y}\; \psi_{j_x, j_y, i_x, i_y}(x, y) \qquad (4.16)$$

with $d_{j_x, j_y, i_x, i_y} = <f, \psi_{j_x, j_y, i_x, i_y}>$. However in this basis the two variables x and y are dilated separately and therefore no longer form a multiresolution analysis. This means that the functions ψ_{j_x, j_y} involve two scales, 2^{j_x} and 2^{j_y}, and each of the functions is essentially supported on a rectangle with these side lengths. Hence the decomposition is often called rectangular wavelet decomposition. This is closely related to the standard form of operators using the nomenclature of Beylkin [3]. From the algorithmic viewpoint this is equivalent to apply the one–dimensional wavelet transform to the rows and the columns of a matrix representing an operator or a two–dimensional function. For some applications such a basis is advantageous,

for others not. For exemple in turbulence the notion of a scale has an important meaning and one would like to have a unique scale assigned to each basis function.

4.2.2   2D Multi-Resolution Analysis

A suitable concept which fulfills the above requirement of having a unique scale is the construction of a truly two-dimensional MRA of $L^2(I\!\!R^2)$. It can be obtained through the tensor product of two one-dimensional MRA's of $L^2(I\!\!R)$ [42]. More precisely one defines the spaces $\mathbf{V}_j, j \in Z\!\!\!Z$ by

$$\mathbf{V}_j = V_j \otimes V_j \qquad (4.17)$$

and $\mathbf{V}_j = \overline{span}\{\phi_{j,i_x,i_y}(x,y) = \phi_{j,i_x}(x)\ \phi_{j,i_y}(y)\ , i_x, i_y \in Z\!\!\!Z\}$ fulfilling analogous properties as in the one–dimensional case (3.1) - (3.4).
Likewise, we define the complement space $\mathbf{W}_j$ to be the orthogonal complement of $\mathbf{V}_j$ in $\mathbf{V}_{j+1}$, *i.e.*

$$\begin{aligned} \mathbf{V}_{j+1} &=& V_{j+1} \otimes V_{j+1} = (V_j \oplus W_j) \otimes (V_j \oplus W_j) \qquad (4.18) \\ &=& V_j \otimes V_j \oplus ((W_j \otimes V_j) \oplus (V_j \otimes W_j) \oplus (W_j \otimes W_j)) \ \ (4.19) \\ &=& \mathbf{V}_j \oplus \mathbf{W}_j \qquad (4.20) \end{aligned}$$

It follows that the orthogonal complement $\mathbf{W}_j = \mathbf{V}_{j+1} \ominus \mathbf{V}_j$ consists of three different types of functions and is generated by three different wavelets

$$\psi^{\kappa}_{j,i_x,i_y}(x,y) = \left\{ \begin{array}{ll} \psi_{j,i_x}(x)\ \phi_{j,i_y}(y) & ;\ \kappa = 1 \\ \phi_{j,i_x}(x)\ \psi_{j,i_y}(y) & ;\ \kappa = 2 \\ \psi_{j,i_x}(x)\ \psi_{j,i_y}(y) & ;\ \kappa = 3 \end{array} \right. \qquad (4.21)$$

Observe that here the scale parameter j simultaneously controlls the dilatation in x and in y. We recall that in d dimensions this construction yields $2^d - 1$ types of wavelets spanning $\mathbf{W}_j$.
Using (4.21) each function $f \in L^2(I\!\!R^2)$ can be developed into an MRA basis as

$$f(x,y) = \sum_j \sum_{i_x,i_y} \sum_{\kappa=1,2,3} d^{\kappa}_{j_x,j_y,i_x,i_y}\ \psi^{\kappa}_{j,i_x,i_y}(x,y) \qquad (4.22)$$

with $d^{\kappa}_{j_x,j_y,i_x,i_y} =< f, \psi^{\kappa}_{j,i_x,i_y} >$. The wavelets $\psi^{\kappa}_{j,i_x,i_y}$ are the basis functions of the so-called square wavelet decomposition. The algorithmic structure of the one-dimensional transforms carries over to the two-dimensional case by simple tensorisation, *i.e.* applying the filters at each decomposition step to rows and columns. Applying this kind of transform to matrices representing operators (differential, integral, integro-differential) leads to the non-standard form in the terminology of Beylkin [3].

Remark:

The described two-dimensional wavelets and scaling functions are separable. This advantage facilitates the generation of a multidimensional MRA from several one-dimensional MRA's. However the main drawback of this construction is that three wavelets are needed to span the orthogonal complement space $\mathbf{W}_j$ in two dimensions and seven in three dimensions. Another property should be mentioned. By construction the wavelets are anisotropic, *i.e.* horizontal, diagonal and vertical directions are preferred. This could be an advantage in digital signal processing to recognize corners and edges.

4.2.3   Periodic 2D Multi-Resolution Analysis

Using the tensor product construction of two-dimensional wavelets on the real line and the periodization technique, see *e.g.* [46], we now recall the essential features of periodic two-dimensional wavelets of $L^2(\mathbb{T}^2)$. For notational ease we drop from now on the tilde introduced to distinguish the periodic wavelets from those on the real line. In the latter applications the periodic basis is used throughout unless otherwise explicitly stated.
A two-dimensional MRA of $L^2(\mathbb{T}^2)$ is a sequence of embedded subspaces $\mathbf{V}_j \subset \mathbf{V}_{j+1}$, $j \in \mathbb{N}_0$. It can be obtained through the tensor product of two one–dimensional MRA's of $L^2(\mathbb{T})$ [42]. This induces a decomposition of $L^2(\mathbb{T}^2)$ into mutually orthogonal hierarchical subspaces

$$L^2(\mathbb{T}^2) = \mathbf{V}_0 \oplus_{j \geq 0} \mathbf{W}_j \qquad (4.23)$$

The space $\mathbf{V}_j$ is generated by the bivariate scaling functions

$$\mathbf{V}_j = \overline{span} \left\{ \phi_{j,i_x,i_y}(x,y) \; = \; \phi_{j,i_x}(x) \, \phi_{j,i_y}(y) \right\}_{i_x,i_y=0,\dots,2^j-1} \qquad (4.24)$$

and the orthogonal complement space $\mathbf{W}_j \; = \; \mathbf{V}_{j+1} \ominus \mathbf{V}_j$, $j \geq 0$ by three different wavelets

$$\mathbf{W}_j = \overline{span} \left\{ \psi^{\kappa}_{j,i_x,i_y}(x,y) \right\}_{i_x,i_y=0,\dots,2^j-1, \kappa=1,2,3} \qquad (4.25)$$

with $\psi^{\kappa}_{j,i_x,i_y}$ defined as in (4.21) using the periodic analogons.
Correspondingly, any function $f \in L^2(\mathbb{T}^2)$ which is at least continuous can be projected onto $\mathbf{V}_J$ by collocation

$$f_J(x,y) \; = \; \sum_{i_x=0}^{2^J-1} \sum_{i_y=0}^{2^J-1} \; f\left(\frac{i_x}{2^J}, \frac{i_y}{2^J}\right) \, S_{J,i_x,i_y}(x,y) \qquad (4.26)$$

using the two-dimensional cardinal Lagrange function

$$S_{j,i_x,i_y}(x,y) = S_{j,i_x}(x) S_{j,i_y}(y) \quad . \qquad (4.27)$$

It can then be expressed as

$$f_J(x,y) = c_{0,0,0}\, \phi_{0,0,0}(x,y) \;+\; \sum_{j=0}^{J-1}\sum_{i_x=0}^{2^j-1}\sum_{i_y=0}^{2^j-1}\sum_{\kappa=1}^{3} d^\kappa_{j,i_x,i_y}\, \psi^\kappa_{j,i_x,i_y}(x,y)$$

$$(4.28)$$

with coefficients

$$d^\kappa_{j,i_x,i_y} = \langle f,\, \psi^\kappa_{j,i_x,i_y}\rangle\,, \qquad c_{0,0,0} = \int_{\mathbb{T}^2} f(x,y)\, dx\, dy. \qquad (4.29)$$

using that $\phi_{0,0,0} = 1$.

Representing a function in terms of wavelet coefficients has the following advantages. Smooth functions yield rapid decay of the coefficients in scale (depending on the number of vanishing moments of ψ_{ji}). At locations where u develops a singularity or an 'almost singularity' only local coefficients have to be retained (depending on the decay of ψ_{ji} in space). Second, all employed basis functions are mutually orthogonal, a property which is the keystone of the algorithms.

4.3   Algorithm

In case of a regular sampling and periodic functions, computations can be done in physical space by periodizing the required filters (defined below) using Mallat's algorithm [39]. For long filters it is more economical, however, to use fast convolution in Fourier space employing FFT. Following [46] we describe such a transformation together with a computational trick for its acceleration [26]. The algorithm is based on the application of three discrete filters. The scaling coefficients $c_{J,k}$ are computed by application of the interpolation filter

$$I_n^J = \langle S_{J,n}, \phi_{J,0}\rangle\,, \quad \widehat{I^J} = 2^{-3J/2}\,\widehat{I}(\frac{k}{2^j})\,, \quad \widehat{I}(k) = \widehat{S}(k)/\widehat{\phi}(k) \qquad (4.30)$$

to the sampled values $\{f(\frac{i}{2^J})\}_i$.
    The filters

$$G_n^j = \langle \phi_{j,n}, \psi_{j-1,0}\rangle\,, \qquad H_n^j = \langle \phi_{j,n}, \phi_{j-1,0}\rangle \qquad (4.31)$$

are classically used for computing the wavelet transform. They can be obtained in physical space for compactly supported bases and in Fourier space through

$$\widehat{H}(k) = \widehat{\phi}(2k)/\widehat{\phi}(k) \quad, \qquad \widehat{G}(k) = \widehat{\psi}(2k)/\widehat{\phi}(k) \qquad (4.32)$$

    The algorithm then reads

step 0. FFT of the values $\{f_i\}_{i=0,\ldots,2^J-1}$ at the points $\{x_i = \frac{i}{2^J}\}_{i=0,\ldots,2^J-1}$
to the
Fourier coefficients $\{\widehat{f}_k\}_{k=0,\ldots,2^J-1}$.

step 1. Interpolation using the Lagrange function $S_J(x)$ of the space V_J
by computation in Fourier space : application of $\widehat{I}_J$ gives $(\widehat{\overline{f}_J})_k$, $k = 0,\ldots,2^J-1$.

step 2. Application of Filters G and H in Fourier space (* indicating double length sequences)

$$(\widehat{\overline{f}^*_{J-1}})_k = \overline{\widehat{H}_k}\,(\widehat{\overline{f}_J})_k \qquad k = 0,\ldots,2^J-1 \qquad (4.33)$$

$$(\widehat{\tilde{f}^*_{J-1}})_k = \overline{\widehat{G}_k}\,(\widehat{\tilde{f}_J})_k \qquad k = 0,\ldots,2^J-1 \qquad (4.34)$$

step 3. Instead of setting

$$\overline{f}_{J-1,i} = \overline{f}^*_{J-1,2i} \qquad \tilde{f}_{J-1,i} = \tilde{f}^*_{J-1,2i} \qquad i = 0,\ldots,2^{J-1}-1 \quad (4.35)$$

in physical space, downsampling can be done directly in Fourier space through

$$(\widehat{\overline{f}_{J-1}})_k = (\widehat{\overline{f}^*_{J-1}})_k + (\widehat{\overline{f}^*_{J-1}})_{k+2^{J-1}} \qquad k = 0,\ldots,2^{J-1} \qquad (4.36)$$

$$(\widehat{\tilde{f}_{J-1}})_k = (\widehat{\tilde{f}^*_{J-1}})_k + (\widehat{\tilde{f}^*_{J-1}})_{k+2^{J-1}} \qquad k = 0,\ldots,2^{J-1} \qquad (4.37)$$

step 4. Inverse FFT of lenght 2^{J-1} to get $\{\tilde{f}_{J-1,i}\}_{i=0,\ldots,2^{J-1}-1}$.

iterate steps 2 to 4 replacing J by $j = J-1,\ldots,0$. Observe that in the last step 2^{-1} is replaced by 0 and $(\widehat{\overline{f}_0})_0 = \overline{f}_{0,0}$.

The use of (4.36), (4.37) instead of (4.35) leads to a speed up by a factor 6 with respect to extracting the coefficients in physical space. The inverse transform is obtained by executing the above steps in reversed order omitting the conjugate complex in (4.33), (4.34) and replacing step 3 with upsampling in Fourier space.

Part II
Statistical Analysis

5   Classical tools

5.1   Methodology

Turbulence research is based on either laboratory or numerical experiments. Typical quantities measured to characterize turbulent flows are scalar fields (temperature, concentration, pressure, etc), vector fields (velocity, vorticity, etc), tensor fields (stress, strain, etc).

5.1.1   Laboratory experiments

Laboratory experiments are done (*e.g.* in wind tunnels or water tank) using flow visualisations and time measurements performed in few points of the flow (*e.g.* hot-wire anemometry, laser velocimetry). Flow visualizations give mostly qualitative information. Time measurements give quantitative information by accumulating well-sampled and well-converged time statistics, although only at very few spatial locations. By checking Taylor's hypothesis, namely that the time fluctuations are small compared to the mean flow velocity, one assumes that the time statistics can be identified with the space statistics. This allows to compare laboratory measurements with the predictions of the statistical theory of turbulence, and also with the statistics obtained from numerical experiments.

5.1.2   Numerical experiments

Numerical experiments are based on the accepted assumption that Navier–Stokes is the fundamental equation of fluid dynamics whatever the flow regime. The turbulent regime is reached when the nonlinear advective term dominates the linear dissipative term (limit $\nu \to 0$ or $Re \propto 1/\nu \to \infty$). In this highly nonlinear regime, Navier–Stokes solutions can only be computed by numerical approximation. The computation predicts the time evolution of one flow realization only. Statistical analyses are performed afterwards in three different ways:

- by computing spatial statistics of instanteneous turbulent fields, which is valid only if the computational domain is much larger than the integral scale where turbulence is produced,

- by computing time statistics of long flow history, which is valid only if the time evolution is much larger than the eddy turn over time characteristic of turbulent flow instabilities,

- by running a large number of numerical simulations for the same pa-
  rameter and flow configuration, but with different initial conditions.
  The ensemble averages are computed afterwards. This procedure re-
  quires a number of independant realisations sufficient to ensure the
  stationarity of the probability distribution.

5.2   Averaging procedure

Turbulent flows are characterized by their unpredictability, namely each
flow realization is different, although the statistics are reproducible as long
as the flow configuration and parameters are the same. This is the reason
why turbulence models predict only statistical quantities.

Another essential characteristic of turbulent flows is their intermittency,
i.e. the fact that we observe in each flow realization well localized strong
events (bursts). This intermittent behaviour is not very pronounced in
the velocity field, but becomes dominant when one considers the velocity
gradients or the vorticity fields. They are characterized by non-Gaussian
probability distribution functions, whose tails correspond to the intermit-
tent bursts. We think that the flow intermittency comes from the nonlinear
dynamics of turbulent flows which, for incompressible fluids, tend to form
well localized coherent vortices (vortex spots in two dimensions and vortex
tubes in three dimensions) which move around in a chaotic way resulting
from their mutual interactions.

A crucial difficulty in turbulence modelling is to define averages able
to take into account intermittency. Actually the L^2-norm averages, *i.e.*
$(\int |f(x)|^2 dx)^{1/2}$), classically used in turbulence (*e.g.* two-point correlations,
second order structure functions, spectra) are 'blind' to intermittency, be-
cause the well localized strong events responsible for intermittency are too
rare to affect the L^2-norm, their weight remaining negligible in the integral.

To define averages able to take into account intermittency there are two
possible strategies:

- either to consider L^p-norms, *i.e.* $((\int |f(x)|^p dx)^{1/p})$ with p large enou-
  gh to have the values of the PDF tails (Probability Distribution Func-
  tion) contributing significantly to the integral,

- or to extract the rare (intermittent) events, responsible for the heavy
  tails of the PDF, from the dense (non-intermittent) events, which
  contribute only to the center of the PDF, and perform classical L^2-
  norm averages for the dense events only.

The second approach corresponds to conditional averages and requires
a criterium to separate the rare events from the dense events. As we have
assumed that the intermittency of turbulent flows is due to the presence of

coherent vortices, responsible for the rare events, we first need to identify them in order to then be able to extract them.

As we have shown [17], [15] the coherent vortices can be characterized by the fact that they correpond to the strongest wavelet coefficients of the vorticity field. Based on this property we have defined a procedure to extract them [19], [21], which consists in retaining only those vorticity wavelet coefficients $\tilde{\omega}$ which are larger than a threshold value $\tilde{\omega}_T = (2Z \log_{10} N)^{1/2}$, with Z the total enstrophy and N the resolution (*i.e.* the number of grid points or wavelet coefficients). We then verify that the PDF of the discarded coefficients, *i.e.* those smaller than the treshold $\tilde{\omega}_T$ which correspond to the dense non-intermittent events, is actually Gaussian.

5.3 Statistical diagnostics

5.3.1   Probability Distribution Function (PDF)

To motivate the introduction of a probability space $(\Xi, \mathcal{F}, \mathcal{P})$ we consider:

- the set of all possible configurations of the flow, *i.e.* the phase space of the Navier–Stokes equations, denoted by Ξ,

- the collection $\mathcal{F}$ of all experiments with a definite outcome which have been performed, called the flow realisations,

- a probability measure $\mathcal{P}$ assigned to $\mathcal{F}$, such that $\mathcal{P}(\emptyset) = 0$ and $\mathcal{P}(\Xi) = 1$, which assigns a probability to each experiment which has been performed.

We consider a stationary, homogeneous and isotropic random field $f(\xi, \vec{x}, t) \in \mathcal{F}$, with $\xi \in \Xi$, $\vec{x} \in I\!\!R^n$ and $t \in I\!\!R_0^+$. For fixed ξ the function $f(\vec{x}, t)$ is called a realization of the random field or a sample, *e.g.* one component of the velocity field.

Definition of the PDF:
Using the probability measure $\mathcal{P}$ we define the distribution function $F(g) = \mathcal{P}(-\infty < f \leq g,\ f \in \Xi)$ which measures the probability of f having a value less or equal to g.

5.3.2   Radon-Nikodyn's theorem

If the probability measure $\mathcal{P}$ is absolutely continuous, there exists a probability density p of $\mathcal{P}$ such that $p(f) = \frac{d\mathcal{P}}{df}$, which corresponds to the derivative $\frac{dF}{dg}$ of the distribution F, *i.e.* $p(f)df = \mathcal{P}(f < g \leq f + df,\ g \in \Xi)$.

The probability density is normalized such that $\int_{I\!\!R} p(x)\, dx = 1$.

5.3.3 Definition of the joint probability

Let f and g be two random fields, one can define the joint probability

$$F(f,g) = \mathcal{P}(-\infty < f' \le f, \ -\infty < g' \le g, \ [f',g'] \in \Xi).$$

The corresponding joint probability density function is given by $p(f,g) = p(f)p(g) - p(f \cap g)$ (Bayes' theorem). If f and g are independent and identically distributed (i.i.d.), then $p(f,g) = p(f)p(g)$.

5.3.4 Statistical moments

The q-th order moments of the random field f are defined as

$$M_q(f) = \langle f^q \rangle = \int f^q \, p(f) \, df \qquad (5.1)$$

If $f \in \Xi$ is ergodic the moments can also be expressed as space averages

$$M_q(f) = \int (f(\vec{x}))^q \, d^n\vec{x}, \qquad (5.2)$$

where the integral is defined as

$$\int = \lim_{L \to \infty} \frac{1}{L^3} \int_0^L \int_0^L \int_0^L, \qquad (5.3)$$

L being the size of the domain.

Ratios of moments are defined, such as

$$Q_{p,q}(f) = \frac{M_p(f)}{(M_q(f))^{p/q}} \qquad (5.4)$$

Classically one chooses $q = 2$, which leads to define statistical quantitities such as:

- skewness $S = Q_{3,2}(f)$,
- flatness $F = Q_{4,2}(f)$,
- hyperskewness $S_h = Q_{5,2}(f)$
- hyperflatness $F_h = Q_{6,2}(f)$.

5.3.5 Structure functions

The p–th order structure function of a random scalar field f is defined as

$$S_{p,f}(\vec{l}) = \int (f(\vec{x}+\vec{l}) - f(\vec{x}))^p \, d^n\vec{x}. \qquad (5.5)$$

5.3.6 Autocorrelation function

The autocorrelation function of the random scalar field f is defined as

$$R(\vec{l}) = \int f(\vec{x}) f(\vec{x} + \vec{l}) \, d^n \vec{x} \qquad (5.6)$$

and for vector fields $\vec{f}$ we get the two–point correlation tensor

$$R_{ij}(\vec{l}) = \int f_i(\vec{x}) f_j(\vec{x} + \vec{l}) \, d^n \vec{x} \qquad (5.7)$$

Note that in turbulence the above quantity computed for the velocity field is called Reynolds stress tensor, and plays a key role in turbulence modelling.

5.3.7 Fourier spectrum

Definition of the spectrum:
The spectrum of the random scalar field f is the Fourier transform of its autocorrelation function:

$$\Phi(\vec{k}) = \frac{1}{(2\pi)^n} \int R(\vec{l}) \, e^{-i\vec{k}\cdot\vec{l}} \, d^n \vec{l} \qquad (5.8)$$

For vector fields we obtain analogously

$$\Phi_{ij}(\vec{k}) = \frac{1}{(2\pi)^n} \int R_{ij}(\vec{l}) \, e^{-i\vec{k}\cdot\vec{l}} \, d^n \vec{l} \qquad (5.9)$$

One can integrate $\Phi(\vec{k})$ on shells of radius $k = |\vec{k}|$ which gives the one-dimensional spectrum

$$E(k) = \int \Phi(\vec{k}) \, k^{n-1} \, d\theta . \qquad (5.10)$$

5.3.8 Wiener-Khinchin's theorem

For a function $R(l) \in L^1(\mathbb{R})$, to be the correlation function of a homogeneous field $f(x)$ which satisfies the condition $S_2(l) \to 0$ for $l \to 0$, it is necessary and sufficient that it has a representation of the form $R(l) = \int_{\mathbb{R}} E(k) \, e^{ikl} \, dk$ where $E(k) \geq 0$ is the spectral density of the random variable $f(x)$.

Remark:
If $R(l)$ is not in $L^1(\mathbb{R})$, then Wiener-Khinchin holds in a distributional sense only, *e.g.* for a Gaussian white noise $R(l) = \delta_{l,0}$ therefore it is not in L^1 and $E(k) = 1$.

The spectrum $E(k)$, the second order structure function $S_{2,f}(l)$ and the autocorrelation function $R(l)$ fulfill the following relations:

$$R(l) \;=\; \int f(x+l)f(x)\,dx \;=\; 2\int_0^\infty \cos(2\pi kl)E(k)dk \qquad (5.11)$$

and hence we get

$$S_{2,f}(l) = \langle (f(x+l)-f(x))^2 \rangle = 2R(0)-2R(l) = 2\int_0^\infty (1-\cos(2\pi kl))E(k)dk$$
$$(5.12)$$

Remark:
The above relation illustrates that the structure function corresponds to a high pass filtered spectrum although the corresponding filter is not very selective. We will propose wavelet tools to improve the filter selectivity.

6   Statistical tools based on the continuous wavelet transform

6.1   Local and global wavelet spectra

When analyzing velocity signals of turbulent flows one should calculate ensemble averages of the energy spectra from many realizations. In practice, to avoid performing ensemble averages, one assumes ergodicity of the turbulent motions and averages only one flow realization split into many pieces whose lengths are larger than the integral scale (which is the largest correlated scale in a turbulent signal). In statistical theory of homogeneous turbulence, only the modulus of the Fourier transform is used (*e.g.* the energy spectrum) and thus the phase information is lost. This is probably a major weakness of the traditional way of analyzing turbulence since it neglects any spatial organization of the turbulent fields, which happens in each flow realization although the averages are homogeneous. For statistically inhomogeneous flows the standard statistical tools, *e.g.* the energy spectrum which is the Fourier transform of the two-point correlation of the velocity increments, are too limited to analyze and model turbulence.

The wavelet transform extends the concept of energy spectrum so that one can define a local energy spectrum $\tilde{E}(x,k)$ using the wavelet transform (which, as we have seen conserves, the L^2–norm of a function), such that

$$\tilde{E}(k,x) = \frac{1}{2C_\psi k_\psi} \left| \tilde{f}\left(\frac{k_\psi}{k}, x \right) \right|^2 \quad \text{for} \quad k \geq 0 \qquad (6.1)$$

where k_ψ is the peak wave number of the analyzing wavelet ψ and C_ψ as defined in (3.1). By measuring $\tilde{E}(k,x)$ at different places in a turbulent flow one might estimate what parts of the flow contribute most to the overall Fourier energy spectrum and how the energy spectrum depends on local flow

conditions. For example, one can determine the type of energy spectrum contributed by coherent structures, such as isolated vortices, and the type of energy spectrum contributed by the unorganized part of the flow.

Although the wavelet transform analyses the flow into wavelets rather than complex exponentials one shows [47] that the mean wavelet energy spectrum converges to the Fourier energy spectrum provided the analyzing wavelets have enough cancellations. More precisely the mean wavelet spectrum $\tilde{E}(k)$

$$\tilde{E}(k) = \int_0^{+\infty} \tilde{E}(k, x) dx \qquad (6.2)$$

gives the correct Fourier exponent for a power-law Fourier energy spectrum $E(k) \propto k^{-\beta}$ if the analysing wavelet has at least $n > (\beta - 1)/2$ vanishing moments. This condition is the same as that for detecting singularities derived in the previous section since $\beta = 1 + 2\alpha$ for isolated cusps. Thus, the steeper the energy spectrum the more vanishing moments of the wavelet we need. The inertial range in turbulence has a power-law form. The ability to correctly characterize power-law energy spectra is therefore a very important property of the wavelet transform (which is related to its ability to detect and characterize singularities).

6.2   Relation with Fourier spectrum

The mean wavelet energy spectrum $\tilde{E}(k)$ is a smoothed version of the Fourier energy spectrum $E(k)$. This can be seen from the following relation between the two spectra

$$\tilde{E}(k) = \frac{1}{2C_\psi k_0} \int_0^{+\infty} E(k') \left| \hat{\psi}\left(\frac{k_0 k'}{k}\right) \right|^2 dk' \qquad (6.3)$$

which shows that the mean wavelet spectrum is an average of the Fourier spectrum weighted by the square of the Fourier transform of the analysing wavelet shifted at wavenumber k. Note that the larger k is, the larger the averaging interval, because wavelets are bandpass filters at $\frac{\Delta k}{k}$ constant. This property of the mean wavelet energy spectrum is particularly useful for turbulent flows. Indeed, the Fourier energy spectrum of a single realization of a turbulent flow is too spiky to be able to clearly detects a slope, but it is no more the case for the mean wavelet energy spectrum which is much smoother.

The Mexican hat wavelet

$$\hat{\psi}(k) = k^2 \exp(-k^2/2) \qquad (6.4)$$

has only two vanishing moments and thus can correctly measure energy spectrum exponents up to $\beta < 5$. Only the zeroth order moment of the

Morlet wavelet

$$\begin{aligned}
\hat{\psi}(k) &= \frac{1}{2\pi}\exp(-(k - k_\psi)^2/2) \quad \text{for} \quad k > 0 \\
\hat{\psi}(k) &= 0 \quad \text{for} \quad k \le 0
\end{aligned} \tag{6.5}$$

is zero, but the higher n^{th} order moments are very small ($\propto k_\psi^n \exp(-k_\psi^2/2)$) provided that k_ψ is sufficiently large. Therefore the Morlet wavelet transform gives accurate estimates of the power–law exponent of the energy spectrum at least for approximately $\beta < 7$ (if $k_\psi = 6$).

There is also a family of wavelets [47] with an infinite number of cancellations

$$\hat{\psi}_n(k) = \alpha_n \exp\left(-\frac{1}{2}\left(k^2 + \frac{1}{k^{2n}}\right)\right), \quad n \ge 1, \tag{6.6}$$

where α_n is chosen for normalization. The wavelets defined in (6.6) can therefore correctly measure any power–law energy spectrum. Furthermore, these wavelets can detect the difference between a power–law energy spectrum and a Gaussian energy spectrum ($E(k) \propto \exp(-(k/k_0)^2)$). It is important to be able to determine at what wavenumber the power–law energy spectrum becomes exponential since this wavenumber defines the end of the inertial range of turbulence and the beginning of the dissipative range.

6.3   Application to turbulence

The first measurements of local energy spectra in turbulence were reported in [18] and [40]. Farge et al. [18] used a Morlet wavelet to obtain the local and global energy spectra for a 3D mixing layer computed by DNS. They showed that the deviation from the mean energy spectrum was very large due to intermittency and increased with the scales. Therefore they conjectured that the intermittency of the flow increases for increasing Re. Meneveau [40] used the discrete wavelet transform to measure local energy spectra in experimental and Direct Numerical Simulation (DNS) flows. He found that the standard deviation of the local energy (a measure of the spatial fluctuation of energy) was approximately 100% throughout the inertial range. He also calculated the spatial fluctuation of $T(k)$ which measures the transfer of energy from all wavenumbers to wavenumber k. On average $T(k)$ is negative for the large scales and positive for the small scales, indicating that in three-dimensional turbulence energy is, in average, transferred from the large scales to the small scales where it is dissipated. However, he found that at many locations in the flow the energy cascade actually operates in the opposite direction, from small to large scales, indicating a local inverse energy cascade (called back-scattering) which concerns a very important part of the transferred energy. This local spectral information, which links the physical and Fourier representations of turbulence, can be obtained using the wavelet transform but not with the Fourier transform.

7   Statistical tools based on the orthogonal wavelet transform

7.1   Local and global wavelet spectra

In this section we describe some statistical tools based on the orthogonal wavelet transform. We present them considering, as example, a two–dimensional scalar field $f(\vec{x})$ which has vanishing mean and is periodic (the extention to higher dimensions and vector fields is straightforward [54]). Hence we employ a periodic two-dimensional Multi-Resolution Analysis (MRA) [42], [14] and develop the field f, sampled on $N^2 = 2^{2J}$ points, as an orthonormal wavelet series from the largest scale $l_{max} = 2^0$ to the smallest scale $l_{min} = 2^{-J}$:

$$f(x, y) = \sum_{j=0}^{J-1} \sum_{i_x=0}^{2^j-1} \sum_{i_y=0}^{2^j-1} \sum_{\kappa=1}^{3} \tilde{f}^{\kappa}_{j,i_x,i_y} \, \psi^{\kappa}_{j,i_x,i_y}(x, y) \quad , \qquad (7.1)$$

with

$$\psi^{\kappa}_{j,i_x,i_y}(x, y) = \begin{cases} \psi_{j,i_x}(x) \, \phi_{j,i_y}(y) & ; \ \kappa = 1 \quad , \\ \phi_{j,i_x}(x) \, \psi_{j,i_y}(y) & ; \ \kappa = 2 \quad , \\ \psi_{j,i_x}(x) \, \psi_{j,i_y}(y) & ; \ \kappa = 3 \quad , \end{cases} \qquad (7.2)$$

where $\phi_{j,i}$ and $\psi_{j,i}$ are the 2π-periodic one-dimensional scaling function and the corresponding wavelet, respectively. The wavelets $\psi^{\kappa}_{j,i_x,i_y}$ correspond to horizontal, vertical and diagonal directions, for $\kappa = 1, 2, 3$, respectively. Due to orthogonality the coefficients are given by $\tilde{f}^{\kappa}_{j,i_x,i_y} = \langle f , \psi^{\kappa}_{j,i_x,i_y} \rangle$ where $\langle \cdot, \cdot \rangle$ denotes the L^2 inner product.

We can define the scale distribution of energy, also called scalogram, as

$$E_j = \sum_{i_x=0}^{2^j-1} \sum_{i_y=0}^{2^j-1} \sum_{\kappa=1}^{3} |\tilde{f}^{\kappa}_{j,i_x,i_y}|^2 \ . \qquad (7.3)$$

Introducing the discrete mean square wavelet coefficient at scale 2^{-j} and at position $x_{i_x,i_y} = 2^{-j}(i_x + 1/2, i_y + 1/2)$ as

$$\overline{\tilde{f}}(2^{-j}, 2^{-j}(i_x, i_y)) = $$
$$\frac{1}{2}((\tilde{f}^1_{j,i_x,i_y})^2 + (\tilde{f}^1_{j,i_x+1,i_y})^2) + \frac{1}{2}((\tilde{f}^2_{j,i_x,i_y})^2 + (\tilde{f}^2_{j,i_x,i_y+1})^2) + (\tilde{f}^3_{j,i_x,i_y})^2 \ (7.4)$$

we define a discrete local wavelet spectrum [10] by

$$\widetilde{E}(k_j, x_{i_x,i_y}) = \overline{\tilde{f}}(2^{-j}, 2^{-j}(i_x, i_y)) \frac{2^{2j}}{\Delta k_j} \ . \qquad (7.5)$$

This quantitiy allows to study the space dependent spectral behaviour of f. By construction we have

$$\widetilde{E}(k_j) \;=\; \sum_{i_x=0}^{2^j-1} \sum_{i_y=0}^{2^j-1} \widetilde{E}(k_j, x_{i_x,i_y})\,. \tag{7.6}$$

7.2 Relation with Fourier spectrum

Owing to the orthogonality of the wavelet decomposition, the total energy is preserved and we have $E = \sum_j E_j$. To be able to relate the scale distribution to the Fourier spectrum, we introduce the mean wavenumber k_0 of the wavelet ψ, defined by

$$k_0 \;=\; \frac{\int_0^\infty k|\widehat{\psi}(k)|\,dk}{\int_0^\infty |\widehat{\psi}(k)|\,dk}\,. \tag{7.7}$$

Therewith each scale 2^{-j} of the wavelet ψ_j is related to the mean wavenumber $k_j = k_0 2^j$. With $\Delta k_j = \sqrt{k_j k_{j+1}} - \sqrt{k_j k_{j-1}}$, describing the mean radial wavenumber of the three two–dimensional wavelets ψ^κ_{j,i_x,i_y}, we define the global wavelet spectrum as

$$\widetilde{E}(k_j) \;=\; E_j/\Delta k_j\,. \tag{7.8}$$

which is related with the Fourier energy spectrum by

$$\widetilde{E}(k) \;=\; \frac{1}{k} \int_0^\infty E(k')|\widehat{\psi}(k_0 k'/k)|^2 dk'\,. \tag{7.9}$$

The wavelet spectrum is a smoothed Fourier spectrum weighted with the modulus of the Fourier transform of the analyzing wavelet [47]. Note that for increasing wavenumbers the averaging interval becomes larger [14]. A sufficient condition, guaranteeing the global wavelet spectrum to be able to detect the same power–law behaviour $k^{-\alpha}$ as the Fourier spectrum, is that ψ has enough vanishing moments [47], *i.e.*

$$\int_{-\infty}^{+\infty} x^n \psi(x)\,dx \;=\; 0 \quad \text{for} \quad 0 \le n \le \frac{\alpha-1}{2}\,. \tag{7.10}$$

If this condition is not fulfilled the global wavelet spectrum saturates at the critical cancellation order n and shows a power–law behaviour with a slope not steeper than $-2(n+1)$.

7.3 Intermittency measures

Useful diagnostics to quantify the intermittency of a field are the moments of its wavelet coefficients at different scales j [53,54],

$$M_{p,j}(f) \; = \; \frac{1}{3 \cdot 2^{2j}} \sum_{i_x=0}^{2^j-1} \sum_{i_y=0}^{2^j-1} \sum_{\kappa=1}^{3} |\tilde{f}_{j,i_x,i_y}^{\kappa}|^p \quad . \tag{7.11}$$

The sparsity of the wavelet coefficients at each scale can be measured and the intermittency of the field f can be quantified using ratios of the moments at different scales,

$$Q_{p,q,j}(f) = \frac{M_{p,j}(f)}{(M_{q,j}(f))^{p/q}} \quad , \tag{7.12}$$

which may be interpreted as quotient norms between different L^p- and L^q-spaces, corresponding to Besov spaces. Classically, one chooses $q = 2$ to define typical statistical quantities as a function of scale. Recall that for $p = 4$ we obtain the scale dependent flatness $F_j = Q_{4,2,j}$ which is equal to 3 for a Gaussian white noise at all scales j, which proves that this signal is not intermittent. The scale dependent skewness, hyperflatness and hyperskewness are obtained for $p = 3, 5$ and 6, respectively. For intermittent signals $Q_{p,q,j}$ increases with j.

Part III
Computation

8 Coherent vortex extraction

8.1 CVS filtering

In ([21], [23]) we have proposed a wavelet-based method, called Coherent Vortex Simulation (CVS), to compute turbulent flows for regimes where the coherent vortices dominate the nonlinear dynamics. We first present the CVS filtering, which extracts coherent vortices out of each flow realization. We then describe the CVS computation, which calculates the time evolution of turbulent flows by deterministically computing the dynamics of coherent vortices, in an adaptive wavelet basis, and statistically modelling the effect of the coherent velocity field onto the incoherent background flow.

8.1.1 Vorticity decomposition

We describe the wavelet algorithm to extract coherent vortices out of turbulent flows and consider as example the 3D case (for the 2D case refer

to [21]). We consider the vorticity field $\vec{\omega}(\vec{x}) = \nabla \times \vec{v}$, computed at res-
olution $N = 2^{3J}$, N being the number of grid points and J the number
of octaves. Each component is developed into an orthogonal wavelet series
from the largest scale $l_{max} = 2^0$ to the smallest scale $l_{min} = 2^{J-1}$ using a
3D multi-resolution analysis (MRA) ([8], [14]):

$$\omega(\vec{x}) = \bar{\omega}_{0,0,0} \, \phi_{0,0,0}(\vec{x}) + \sum_{j=0}^{J-1} \sum_{i_x=0}^{2^j-1} \sum_{i_y=0}^{2^j-1} \sum_{i_z=0}^{2^j-1} \sum_{\mu=1}^{2^n-1} \tilde{\omega}_{j,i_x,i_y,i_z}^{\mu} \, \psi_{j,i_x,i_y,i_z}^{\mu}(\vec{x}),$$

(8.1)

with $\quad \phi_{j,i_x,i_y i,i_z}(\vec{x}) = \phi_{j,i_x}(x) \, \phi_{j,i_y}(y) \, \phi_{j,i_z}(z)$, and

$$\psi_{j,i_x,i_y,i_z}^{\mu}(\vec{x}) = \begin{cases} \psi_{j,i_x}(x) \, \phi_{j,i_y}(y) \, \phi_{j,i_z}(z) & ; \mu = 1 \quad , \\ \phi_{j,i_x}(x) \, \psi_{j,i_y}(y) \, \phi_{j,i_z}(z) & ; \mu = 2 \quad , \\ \phi_{j,i_x}(x) \, \phi_{j,i_y}(y) \, \psi_{j,i_z}(z) & ; \mu = 3 \quad , \\ \psi_{j,i_x}(x) \, \phi_{j,i_y}(y) \, \psi_{j,i_z}(z) & ; \mu = 4 \quad , \\ \psi_{j,i_x}(x) \, \psi_{j,i_y}(y) \, \phi_{j,i_z}(z) & ; \mu = 5 \quad , \\ \phi_{j,i_x}(x) \, \psi_{j,i_y}(y) \, \psi_{j,i_z}(z) & ; \mu = 6 \quad , \\ \psi_{j,i_x}(x) \, \psi_{j,i_y}(y) \, \psi_{j,i_z}(z) & ; \mu = 7 \quad , \end{cases}$$

(8.2)

where $\phi_{j,i}$ and $\psi_{j,i}$ are the one-dimensional scaling function and the corre-
sponding wavelet, respectively. Due to orthogonality, the scaling coefficients
are given by $\bar{\omega}_{0,0,0} = \langle \omega \, , \, \phi_{0,0,0} \rangle$ and the wavelet coefficients are given by
$\tilde{\omega}_{j,i_x,i_y,i_z}^{\mu} = \langle \omega \, , \, \psi_{j,i_x,i_y,i_z}^{\mu} \rangle$, where $\langle \cdot, \cdot \rangle$ denotes the L^2-inner product.

8.1.2   Nonlinear thresholding

We then split the vorticity field into $\vec{\omega}_C(\vec{x})$ and $\vec{\omega}_I(\vec{x})$ by applying a non-
linear thresholding to the wavelet coefficients. The threshold is defined as
$\epsilon = (4/3Z \log N)^{1/2}$ and it only depends on the total enstrophy Z and on the
number of grid points N without any adjustable parameters. The choice
of this threshold is based on theorems ([11], [12]) proving optimality of
the wavelet representation to denoise signals in presence of Gaussian white
noise, since this wavelet-based estimator minimizes the maximal L^2-error
for functions with inhomogeneous regularity.

### 8.1.3   Vorticity and velocity reconstruction

The coherent vorticity field $\vec{\omega}_C$ is reconstructed from the wavelet coefficients
whose modulus is larger than ϵ and the incoherent vorticity field $\vec{\omega}_I$ from the
wavelet coefficients whose modulus is smaller or equal to ϵ. The two fields
thus obtained, $\vec{\omega}_C$ and $\vec{\omega}_I$, are orthogonal, which ensures a separation of the
total enstrophy into $Z = Z_C + Z_I$ because the interaction term $\langle \vec{\omega}_C \, , \vec{\omega}_I \rangle$
vanishes. We then use Biot–Savart's relation $\vec{v} = \nabla \times (\nabla^{-2}\vec{\omega})$ to reconstruct
the coherent velocity $\vec{v}_C$ and the incoherent velocity $\vec{v}_I$ for the coherent and
incoherent vorticities respectively.
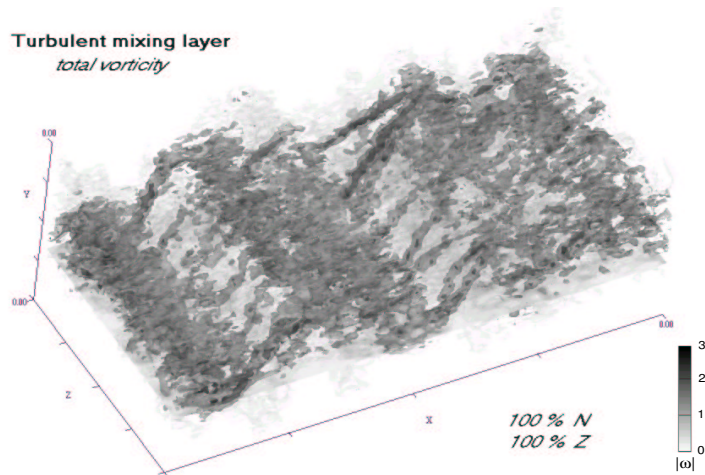
Fig. 2. Total vorticity of the turbulent mixing layer.

8.2   Application to a 3D turbulent mixing layer

In the present lecture notes we apply the above algorithm to a high resolution DNS ($N = 512 \times 256 \times 128$) of a forced turbulent mixing layer [48] to check the potential for the CVS method in 3D shear flows. Fig. 2 show the modulus of vorticity for the total flow. We observe longitudinal vortex tubes, resulting from 3D instability and called ribs, which are wrapped onto four transversal rollers, produced by the 2D Kelvin–Helmholtz instability.
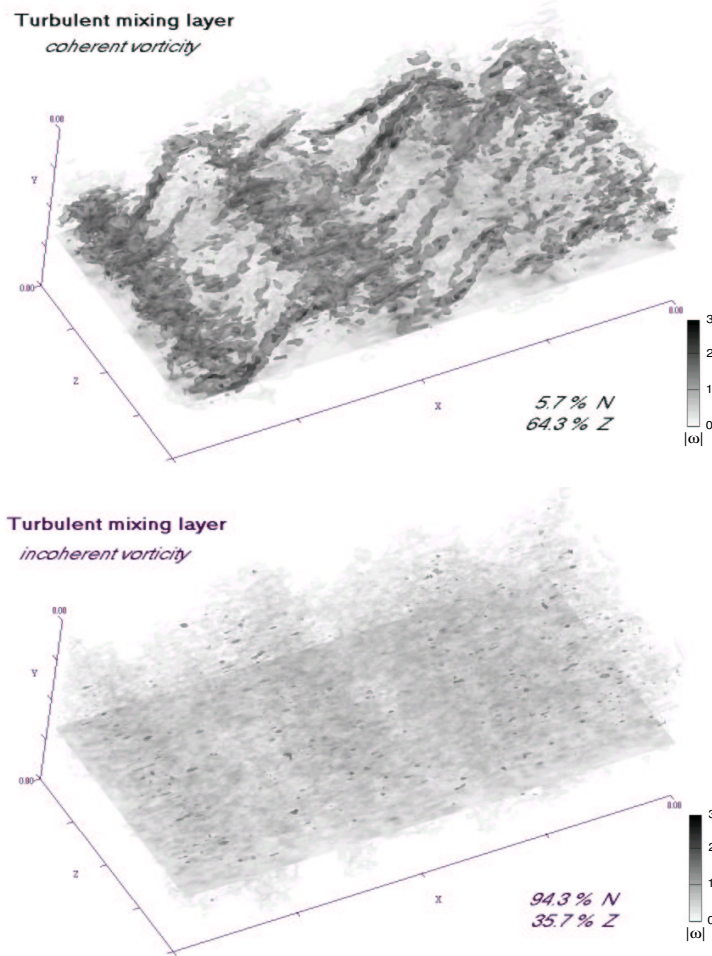
Fig. 3. Top: Coherent vorticity of the turbulent mixing layer reconstructed from 5.7% of the wavelet coefficients and containing 64.3% of the total enstrophy. Bottom: Incoherent vorticity reconstructed from 94.3% of the wavelet coefficients and containing 35.7% of the total enstrophy.

The coherent part (see Fig. 3 top), which represents 3% of the total number of coefficients, captures most of the turbulent kinetic energy and enstrophy, even at high wavenumbers, and the pdf of its vorticity is similar to that of the total flow (see Fig. 4). The incoherent part (see Fig. 3 bottom), which represents 97% of the total number of coefficients, contains little of the turbulent kinetic energy and enstrophy. It is nearly homogenenous with a very low amplitude and contains no structure.

The corresponding 1D energy spectra in the streamwise direction shows that the coherent part presents, all along the inertial range, the same correlation as the total flow, while the incoherent part contains very little energy and is well decorrelated.

8.3 Comparison between CVS and LES filtering

The CVS method is in the spirit of the Large Eddy Simulation (LES) method [24, 37]. But, in contrast to LES, it uses a nonlinear filter that depends on each flow relisation. The CVS filter corresponds to an orthogonal projection, implying $(\vec{\omega}_I)_C = 0$, and is hence idempotent, i.e. $(\vec{\omega}_C)_C = \vec{\omega}_C$, which is not the case for all LES filters (e.g. the Gaussian filter).

In Fig. 4 we compare the CVS and the LES filterings for the same number of retained coefficients ($3\%N$). Since the LES filtering, chosen here to be a Fourier low-pass filter, retains only the low wavenumbers (Fig. 4 top, right), the coherent vortices are smoothed and as a result the variability of vorticity is strongly reduced (see PDF on Fig. 4 bottom, right). In contrast the CVS filtering retains the organized features, whatever their scales are, and as a results the shape of the vorticity PDF is preserved, even for large values of $|\vec{\omega}|$ (Fig. 4 bottom, left).

Concerning turbulence parametrization, i.e. the statistical modelling of the effect of the discarded modes onto the retained modes, for CVS and LES method we can draw the following conclusion:

- The LES filtering has the drawback that the high wavenumber modes are not decorrelated and high amplitudes of vorticity are present. This may lead to nonlinear instabilities which trigger backscatter.

- The CVS filtering allows to disentangle the organized and random components of turbulent flows. As a results the discarded incoherent modes have very weak amplitude, are almost homogeneous in space and are well decorrelated.

In conclusion we conjecture that the derivation of a turbulence model is easier with a CVS filtering than with a LES filtering. However, the CVS filtering requires a dynamically adaptive mesh refinement for solving Navier–Stokes. In the next section we present such a method based on the wavelet representation that we have developed for the 2D Navier–Stokes equations.
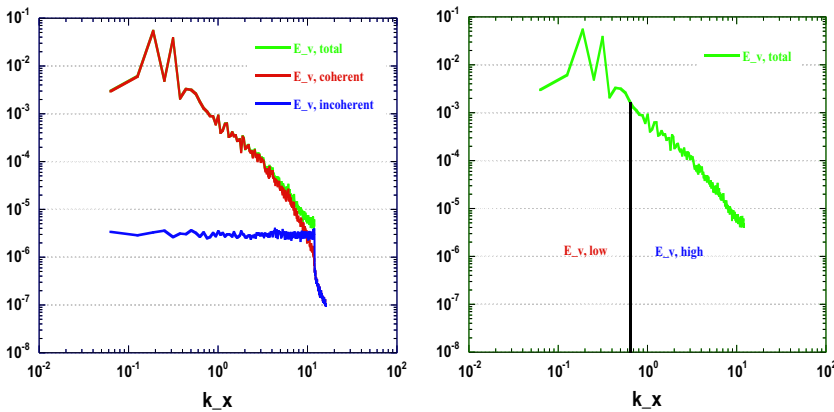
Mixing layer, forced

N = 512 x 256 x 128

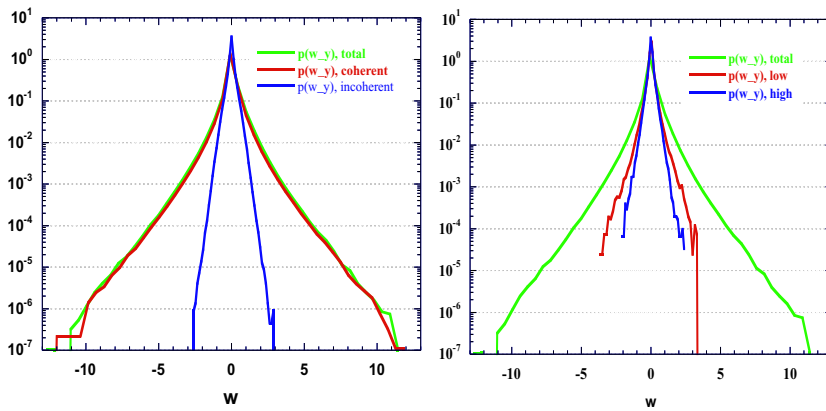| CVS		LES
coherent	3 % N	low wavenumber
incoherent	97 % N	high wavenumber

1D energy spectra E(k_x)

Vorticity PDF p(ω)

Fig. 4. Comparison of CVS (left) with LES (right) filtering. Energy spectra (top) and PDF of vorticity (bottom) of total, coherent and incoherent flow using CVS filtering and of low wavenumber and high wavenumber components using LES filtering.

9   Computation of turbulent flows

9.1   Navier–Stokes equations

9.1.1   Velocity-pressure formulation

The Navier–Stokes equation written in primitive variable formulation (velocity and pressure) describes the dynamics of a Newtonian (deformation proportional to velocity gradients) fluid

$$\partial_t \vec{v} + (\vec{v} \cdot \nabla)\,\vec{v} - \nu\,\nabla^2\,\vec{v} + \frac{1}{\rho}\nabla\,p \;=\; \vec{F} \tag{9.1}$$

and, if we suppose that the fluid is incompressible (constant density of the fluid elements), it is complemented by the continuity equation

$$\nabla \cdot \vec{v} \;=\; 0 \tag{9.2}$$

where $\vec{v} = (v_1(\vec{x}, t), v_2(\vec{x}, t), v_3(\vec{x}, t))$ and $p(\vec{x}, t)$ denote the fluid velocity and the pressure respectively, at point $\vec{x} = (x_1, x_2, x_3)$ and time t. $\vec{F}$ is the field of external forces per unit mass, ρ the density and ν the constant kinematic viscosity. This system of coupled PDE's must be supplemented by appropriate initial and boundary conditions.

9.1.2   Vorticity-velocity formulation

Taking the curl of (9.1), the pressure term can be eliminated and we get a dynamical equation for the vorticity

$$\partial_t \vec{\omega} + (\vec{v} \cdot \nabla)\,\vec{\omega} - \vec{\omega} \cdot \nabla \vec{v} - \nu\,\nabla^2 \vec{\omega} = \nabla \times \vec{F}\,. \tag{9.3}$$

This is an advection-diffusion equation for the vorticity with an additional term $\vec{\omega} \cdot \nabla \vec{v}$, which is responsible for the vortex stretching mechanism, *i.e.* vortex tubes can be stretched by velocity gradients, which leads to vorticity production. In two dimensions this term vanishes, because the vorticity is a pseudo-scalar $\vec{\omega} = (0, 0, \omega_3)$ perpendicular to the velocity gradients.
Taking the divergence of (9.1) and using the incompressibility of $\vec{v}$, we get a Poisson equation for the pressure which is used in many numerical schemes, such as projection methods or fractional step schemes [5], [56]

$$\frac{1}{\rho}\nabla^2\,p \;=\; -\nabla \cdot ((\vec{v} \cdot \nabla)\,\vec{v}). \tag{9.4}$$

The relation $\vec{\omega} \;=\; \nabla \times \vec{v}$ can be inverted for a star shaped domain $\mathcal{D}$ using Poincaré's lemma which leads to:

$$\vec{v} \;=\; -\nabla \times \nabla^{-2}\vec{\omega} \tag{9.5}$$

The above relation can be expressed as a convolution product of the vorticity with an operator K, called the Biot–Savart kernel, *i.e.* $\vec{v} = K \star \vec{\omega}$. As K decays slowly in physical space, *i.e.* as $|\vec{x}|^{-2}$ in three dimensions and as $|\vec{x}|^{-1}$ in two dimensions, the velocity is less localized than the vorticity.

9.2 *Classical numerical methods*

In the last 30 years the progress in numerical methods and the availability of supercomputers have had a significant impact on turbulence research. For example, the importance and role of coherent vortices in three-dimensional turbulence has been established largely by high resolution numerical simulations [1], [57], [58]. Von Neumann's vision, who had suggested in 1949 [45] that turbulence could be simulated numerically, has become a reality. In contrast to the statistical theory of turbulence and to most laboratory experiments, which deal with L^2-norm averaged quantities, numerical experiments deal with non-averaged instantaneous quantities. Numerical experiments deterministically compute the evolution of one flow realization at a time, and perform the desired averages afterwards. There are two ways of computing turbulent flows: either by Direct Numerical Simulation (DNS), or by Modelled Numerical Simulation (MNS).

9.2.1 Direct Numerical Simulation (DNS)

In DNS one computes all degrees of freedom of the flow and both the nonlinear dynamics and the linear dissipation are fully resolved by computing the time evolution of all these degrees of freedom. The DNS schemes currently in use may be classified into three categories:

- Spectral and pseudo-spectral schemes.

- Finite-difference, -volume, and -element methods.

- Lagrangian methods, *e.g.* vortex methods and contour dynamics.

The various methods are characterized by differences in their numerical complexity, accuracy and flexibility. Using DNS the evolution of all scales of turbulent flows can only be calculated for moderate Reynolds numbers with present supercomputers. The severe limit of DNS is that the number of degrees of freedom N for a regular discretization depends on the Reynolds number Re, such that $N \sim Re$ for two-dimensional flows and $N \sim Re^{9/4}$ for the three-dimensional case. At present only moderate Reynolds number flows ($Re \sim 10^3$ in three dimensions) can be simulated using DNS. Although most flows of engineering interest have higher Reynolds numbers ($Re \sim 10^8$), some physical insight can be gained from studying DNS of only moderate Re flows. However, laboratory experiments have shown that new behaviour

appears in the range $Re \sim 10^4 - 10^5$ [9]. As the number of degrees of freedom scales with Reynolds number, the simulation of such high Reynolds number flows in two or three dimensions requires schemes employing some sort of adaptive discretization.

To our knowledge no current non-wavelet DNS methods use a spatial discretization that adapts to the dynamics and structure of the flow. In [30] we have proposed an adaptive wavelet scheme for nonlinear PDE's and we have extended it to the two-dimensional Navier–Stokes equations [28], [51]. Since the wavelet basis functions are localized in both physical and spectral spaces this approach is a compromise between grid-point methods and spectral methods. The adaptive wavelet method is well suited for turbulence simulations because the characteristic structures encountered in turbulent flows are localized coherent vortices evolving under a multiscale nonlinear dynamics. Thus the space- and scale-adaptivity of the wavelet basis should be very efficient at representing turbulence structures and their dynamics. The fact that the basis is adapted to the solution and follows the time evolution of coherent vortices corresponds to a combination of both Eulerian and Lagrangian approaches.

9.2.2   Modelled Numerical Simulation (MNS)

In MNS, *e.g.* Unsteady Reynolds Averaged Navier–Stokes (URANS), LES and nonlinear Galerkin methods, one supposes that many modes can be discarded, provided that some term(s) or some new equation(s) are added to model the effect of the discarded modes onto the retained modes.

The time evolution of the resolved modes is deterministically computed using the same numerical methods as for DNS. Concerning the discarded modes, one supposes that they are slaved to the retained modes and passively follow their motion. Consequently the dynamics of the unresolved modes cannot become unstable and grow in such a way that they would deterministically affect the evolution of the resolved modes. To ensure this one should check that the unresolved modes have reached a statistical equilibrium state and are sufficiently decorrelated. In this case it is no longer necessary to compute the evolution of the unresolved modes in detail because, if they are in statistical equilibrium, their effect onto the retained modes can be entirely characterized by their averages. The model describing the effect of the unresolved modes onto the resolved modes can be specified once the averaged quantities of the unresolved modes can be parametrized as a function of the resolved modes.

Remark:
Ideally, in order to reduce the computational cost as much as possible, the number of resolved modes should be much smaller than the number of discarded modes and should increase more slowly with Re than the total

number of modes does.

9.3   Coherent Vortex Simulation (CVS)

9.3.1   Principle of CVS

Coherent Vortex Simulation (CVS) deterministically computes the evolution of the coherent vorticity $\vec{\omega}_C$ and statistically models the effect of the incoherent vorticity $\vec{\omega}_I$ and velocity $\vec{v}_I$. In the following we apply the CVS method to compute 2D turbulent flows. We filter the two-dimensional Navier–Stokes equations using CVS filtering and obtain the evolution equation for the coherent vorticity ω_C:

$$\partial_t \omega_C + \nabla \cdot (\omega\,\vec{v})_C - \nu\nabla^2 \omega_C \;=\; \nabla \times \vec{F}_C \qquad (9.6)$$
$$\nabla \cdot \vec{v}_C \;=\; 0 \quad .$$

To model the effect of the discarded coefficients, which corresponds to the incoherent stress, we propose (as in LES) to use a Boussinesq ansatz. For the nonlinear term we use Leonard's triple decomposition, because the nonlinear term is computed with the same adapted grid as the linear term (*i.e.* without dealiasing). We decompose the nonlinear term of (9.6) into

$$(\omega\,\vec{v})_C = \omega_C\,\vec{v}_C + L + C + R \quad , \qquad (9.7)$$

where

$$L \;=\; (\omega_C\,\vec{v}_C)_C - \omega_C\,\vec{v}_C \quad ,$$
$$C \;=\; (\omega_I\,\vec{v}_C)_C + (\omega_C\,\vec{v}_I)_C \quad ,$$
$$\text{and} \qquad R \;=\; (\omega_I\,\vec{v}_I)_C \quad ,$$

denoting the Leonard stress L, the cross stress C and the Reynolds stress R, respectively. The sum of these unknown terms corresponds to the incoherent stress:

$$\tau = (\omega\,\vec{v})_C - \omega_C\,\vec{v}_C = L + C + R \quad , \qquad (9.8)$$

which describes the effect of the discarded incoherent terms on the resolved coherent terms. Note that, due to the localization property of the wavelet representation, the Leonard stress L is actually negligible because $(\omega_C\,\vec{v}_C)_C \simeq \omega_C\,\vec{v}_C$ [53].

The filtered Navier–Stokes equations (9.6) can be rewritten as:

$$\partial_t \omega_C + \nabla \cdot (\omega_C\,\vec{v}_C) - \nu\nabla^2 \omega_C \;=\; \nabla \times \vec{F}_C - \nabla \cdot \tau \qquad (9.9)$$
$$\nabla \cdot \vec{v}_C \;=\; 0 \quad .$$

9.3.2   CVS without turbulence model

If we consider a very small threshold, there is no longer any need to model the effect of the incoherent part because the incoherent stress is then negligible, and in this case CVS becomes DNS. Note that even when the wavelet threshold tends to zero, the number of discarded incoherent modes may still be large, due to the excellent compression properties of the wavelet representation for turbulent flows. This is reflected by the fact that many wavelet coefficients are essentially zero and can therefore be discarded without loosing a significant amount of enstrophy.

To obtain the coherent variables ω_C and $\vec{v}_C$ we deterministically integrate (9.6) since the variables are non-Gaussian and correspond to a dynamical system out of statistical equilibrium. We solve these equations in an adaptive wavelet basis [53], [30], [51] (cf. the next section). The separation into coherent and incoherent components is performed at each time step. The adaptive wavelet basis retains only those wavelet modes corresponding to the coherent vortices. It is remapped at each time step in order to follow their motions, in both space and scale. In fact, this numerical scheme combines the advantages of both the Eulerian representation, since it projects the solution onto an orthonormal basis, and the Lagrangian representation, since it follows the coherent vortices by adapting the basis at each time step.

9.3.3   CVS with turbulence model

Up to now no modelling has been done, and equation (9.9) is not closed as long as τ depends on the incoherent unresolved terms. To close it we propose two possibilities to model τ.

- A Boussinesq ansatz as for the LES method:

  we assume that τ is proportional to the negative gradient of the coherent vorticity, *i.e.* $\tau = -\nu_T \, \nabla \omega_C$ with ν_T a turbulent viscosity coefficient. The turbulent viscosity ν_T can be estimated, either using Smagorinsky's model [24], or taking ν_T proportional to the enstrophy fluxes in wavelet space, such that, where enstrophy flows from large to small scales, ν_T is positive, and, where enstrophy flows from small to large scales (*i.e.* backscatter), ν_T becomes negative. This second method for estimating the turbulent viscosity is in the spirit of Germano's dynamical procedure used for LES [24].

- A Gaussian stochastic forcing term:

  we choose τ to be proportional to the incoherent enstrophy Z_I computed at the previous time step. This modelling is made possible since the time evolution of the incoherent background, characterized by the time scale $t_I = (Z_I)^{-1/2}$, is much slower than the characteristic time

scale $t_C = (Z_C)^{-1/2}$ of the coherent motions, because $Z_C \gg Z_I$. This behaviour of the incoherent background had already been noticed, and discussed in comparison to Fourier filtering in [16], [53].

The CVS method relies on the assumption that the incoherent velocity remains Gaussian, which is true as long as the nonlinear interactions between the incoherent modes remains weak. This assumption is valid in regions where the density of coherent vortices is sufficient, because the strain they exert on the incoherent background flow then inhibits the development of any nonlinearity there [34]. However, there may be regions, although small, where the density of coherent vortices is not sufficient to control the incoherent nonlinear term. In this case, there are two solutions:

- To locally refine the wavelet basis in these regions in order to deterministically compute the effect of incoherent nonlinear term (no longer neglected), which will lead to the formation of new coherent vortices by instability of the incoherent background flow.

- To directly model the formation of new coherent vortices by adding locally to the wavelet coefficients the amount of coherent enstrophy which has been transferred from the incoherent enstrophy by the nonlinear instability. This procedure is similar to the wavelet forcing we have proposed in [50].

10   Adaptive wavelet computation

10.1   Adaptive wavelet scheme for nonlinear PDE's

This section presents in a general form the adaptive discretization procedure for nonlinear parabolic PDE's. We consider initial value problems and restrict ourself to periodic boundary conditions. The time discretization is done using a classical finite difference scheme of semi-implicit type. One obtains a set of ODE's or PDE's in space which are then solved at each time step with a method of weighted residuals. The particular choice of the trial and test functions defines the different kinds of integration methods.

We consider nonlinear parabolic evolution equation

$$\partial_t u + Ku - F(u) = 0 \tag{10.1}$$

with an appropriate initial condition $u(t = 0) = u_0$ and periodic boundary conditions. In (10.1) K denotes a linear differential operator in space (*e.g.* $K = -\nabla^2$) and F a nonlinear function of u. Examples fitting in the above framework are the Navier–Stokes or the reaction–diffusion equations.

10.1.1   Time discretization

Equation (10.1) is discretized in time by a semi-implicit finite difference scheme of second order

$$L\,u^{n+1} \;=\; f(u^n, u^{n-1})\,, \tag{10.2}$$

with

$$L \;=\; \gamma\,I +\, K\,, \tag{10.3}$$

$$f \;=\; \frac{4}{3}\,\gamma u^n - \frac{1}{3}\,\gamma u^{n-1} \;+\; F(2\,u^n - u^{n-1}) \tag{10.4}$$

time step Δt, $\gamma = 3/(2\Delta t)$, and I representing the identity. The solution of nonlinear equations is avoided by using an explicit scheme, a modified Adams–Bashforth extrapolation scheme, for the nonlinear function F. However, the restrictive stability condition of a pure explicit scheme is eliminated by discretizing the linear terms $K(u)$ with an implicit scheme of Euler-Backwards type. A suitable first order scheme is employed to start the computation.

The method is presented here considering the equation

$$L\,u \;=\; f \tag{10.5}$$

where L is an elliptic operator with constant coefficients. Typically L is a one or two–dimensional Helmholtz operator ($L = \gamma I - C\partial_{xx}$ or $L = \gamma I - C(\partial_{xx} + \partial_{yy})$), which arises from the time-discretized Navier–Stokes equation, using a semi-implicit scheme.

The symbol representing L in Fourier space is $\sigma(k)$. In the case of the Helmholtz operator we get $\sigma(k) = \gamma I + 4\pi^2 C k^2$ and $\sigma(k_x, k_y) = \gamma I + 4\pi^2 C (k_x^2 + k_y^2)$ for the one and two-dimensional case, respectively. Observe that $\gamma > 0$ yields $\sigma > 0$, which is another way of expressing that L is an elliptic operator with inhomogenous symbol. Hence, in each time step an elliptic problem has to be solved.

10.1.2   Wavelet decomposition

To simplify our presentation we first describe in some detail the spatial wavelet discretization for the one-dimensional case. The complete algorithms together with a mathematical justification can be found in [30].

For the spatial discretization we use a method of weighted residuals (Petrov–Galerkin scheme). The trial functions are orthogonal wavelets and the test functions are operator adapted wavelets, called vaguelettes [38]. To solve the elliptic equation $Lu^{n+1} = f$ at time step t^{n+1} we develop u^{n+1} into an orthogonal wavelet series, i.e. $u^{n+1} = \sum_{ji} \tilde{u}_{ji}^{n+1} \psi_{ji}$. Requiring that

the residuum vanishes with respect to all test functions θ_{kl}, we obtain a linear system for the unknown wavelet coefficients $\tilde{u}_{j,i}^{n+1}$ of the solution u.

$$\sum_{j,i} \tilde{u}_{ji}^{n+1} < L\psi_{ji}, \theta_{kl} > = < f, \theta_{kl} > \qquad (10.6)$$

The test functions θ are defined in such a way that the stiffness matrix $< L\psi_{ji}, \theta_{kl} >$ turns out to be the identity, therefore the solution of equation (10.5) reduces to a simple change of the basis:

$$u^{n+1} = \sum_{kl} < f, \theta_{kl} > \psi_{kl} \qquad (10.7)$$

The right hand side f is then expanded into a biorthogonal vaguelette basis

$$f(x) = \sum_{ji} < f, \theta_{ji} > \mu_{ji}(x) \qquad (10.8)$$

with $\theta_{ji} = L^{\star-1}\psi_{ji}$ and $\mu_{ji} = L\psi_{ji}$ ($\star$ denotes the adjoint operator). By construction θ and μ are biorthogonal, $< \theta_{ji}, \mu_{kl} > = \delta_{j,k}\delta_{i,l}$. We check that θ and μ have actually similar localization properties in physical and in Fourier space as ψ [26] [30].

To get an adaptive space discretization for the problem $Lu^n = f$ we consider only the significant wavelet coefficients of the solution, $u^n = \sum_{ji} \tilde{u}_{ji}^n \psi_{ji}$, i.e. we retain only the coefficients $\tilde{u}_{j,i}^n$ which have an absolute value larger than a given threshold ϵ. Hence the index set of all active wavelet coefficients is restricted to some subset $(j,i) \in \Lambda_{\epsilon}^n$, cf. Fig. 5. The light-grey entries correspond to those wavelet coefficients which are retained for being larger than ϵ.
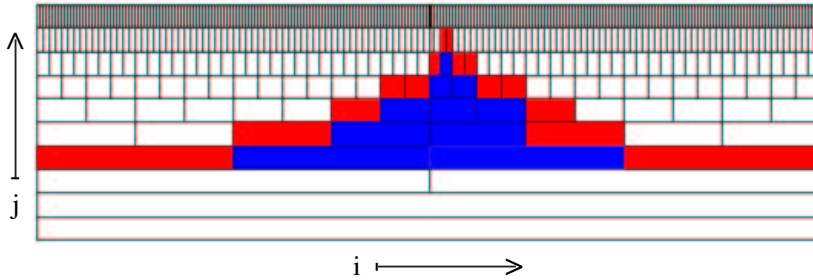
Fig. 5. Scale (vertical axis) and space (horizontal axis) representation of the wavelet coefficients $\tilde{u}_{j,i}$. The light-grey entries correspond to the wavelet coefficients larger than the threshold ϵ. Their neighbors, the dark-grey entries, correspond to the secutity region.

To be able to evolve the equation in time we have to account for the evolution of the solution in wavelet coefficient space. Starting at time step t^n (light-grey entries in Fig. 5) with the index set $\Lambda_\epsilon^n = \{(j, i) \mid |\tilde{u}_{ji}^n| > \epsilon\}$, we switch on all neighbours in wavelet coefficient space (dark-grey entires in Fig. 5) to obtain the new index set Λ_ϵ^{n+1} at time step t^{n+1}. This strategy is performed dynamically as it automatically follows the time evolution of the solution in scale and space. The width of the security region (dark-grey entries in Fig. 5) being added in each time step depends directly on the time sampling Δt which of course has to be sufficiently small (CFL condition) as the nonlinear part of the equation is discretized explicitly.

10.1.3   Evaluation of the nonlinear term

For the evaluation of the nonlinear term $f(u^n)$ in (10.5), where the wavelet coefficients of u^n are given, there are two possibilities.

- Evaluation in wavelet coefficient space:

  This technique is appropriate for simple polynomial nonlinearities, but can be extended to general cases using Taylor series expansion. As illustration we consider a quadratic nonlinear term, *i.e.* $f(u) = u^2$. The wavelet/vaguelette coefficients of f can be calculated using the connection coefficients, *i.e.* one has to calculate the bilinear expression, $\sum_{ji} \sum_{kl} \tilde{u}_{ji} T_{jiklmn} \tilde{u}_{kl}$ with the interaction tensor $T_{jiklmn} = <\psi_{ji} \psi_{kl}, \theta_{mn}>$. Although many coefficients of T are zero or very small, the size of T leads to a computation which is quite untractable in practice.

- Evaluation in physical space:

  This approach is very similar to the pseudo-spectral evaluation of non-linear terms used in spectral methods, and therefore this method is called pseudo–wavelet technique. The advantage of this scheme is that more general nonlinear terms, *e.g.* $f(u) = (1 - u) e^{-C/u}$, can be treated more easily. The prerequesites however are that fast adaptive wavelet decomposition and reconstruction algorithms are available. This means that functions can be reconstructed on a locally refined grid from a sparse set of their significant wavelet coefficients and vice versa. The algorithms are described and analysed in detail in [30]. The method can be summarized as follows: starting from the significant wavelet coefficients of u, *i.e.* $|\tilde{u}_{ji}| > \epsilon$, one reconstructs u on a locally refined grid, $u(x_{kl})$. Then one can evaluate $f(u(x_{kl}))$ pointwise and the wavelet coefficients of f can be calculated using the adaptive decomposition to get $\tilde{f}_{ji}$.

Finally, we have to calculate those scalar products of the r.h.s f with the test functions θ, $\tilde{u}_{ji} = < f, \theta_{ji} >$ for the reduced index set $\{(j, i) \in \Lambda_\epsilon^{n+1}\}$, *i.e.* the dark-grey and the light-grey entries in Fig. 5, to advance the solution in time.

10.1.4   Substraction strategy

The adaptive vaguelette decomposition is based on the hierarchical representation of the r.h.s. We decompose f into

$$f_J = \sum_i < f_J, \theta_{J-1,i} > \mu_{J-1,i} + \sum_i < f_J, \theta_{J-2,i} > \mu_{J-2,i} + \dots \quad (10.9)$$

and introduce then hierarchical grids $x_{Jk} = k/2^J$ (see Fig. 7). Starting with the function values on the locally refined grid $f_J(x_{Jk})$ we calculate first the fine scale wavelet coefficients $\tilde{f}_{J-1,i} = < f_J, \theta_{J-1,i} >$ (Fig. 6) using an interpolatory quadrature rule on the locally refined grid $\{x_{Jk}\}$ (Fig. 7). Then we coarsen the grid and subtract the fine scale contributions of f, *i.e.* we compute $f_{J-1} = f_J - \sum_i \tilde{f}_{J-1,i} \mu_{J-1,i}$ on the grid $\{x_{J-1,k}\}$ (Fig. 7). Hence we get a coarser scale approximation f_{J-1}. Using $f_{J-1}(x_{J-1,k})$ the wavelet coefficients on the next coarser scale $\tilde{f}_{J-2,i} = < f_{J-1}, \theta_{J-2,i} >$ (Fig. 6) can be calculated using the grid $\{x_{J-1,k}\}$ (Fig. 7). The above algorithm is iterated down to the coarsest scale where then a regular grid can be used.
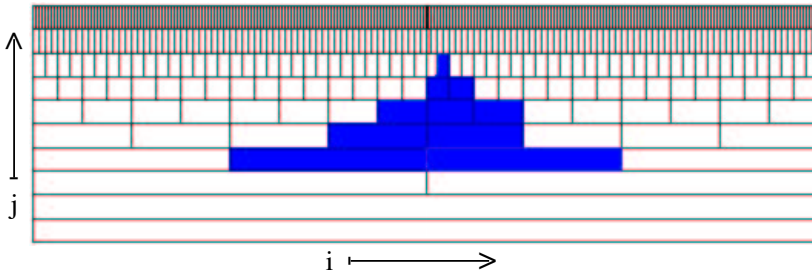
Fig. 6. Scale space representation of the active wavelet coeffcients to be computed (dark entries).
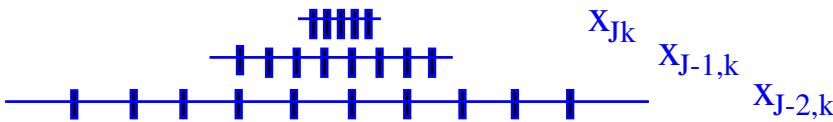
Fig. 7. Corresponding hierarchical grid in physical space.

Remark:
The above algorithm uses the cardinal function $S_{L;J}(x)$ of the operator adapted approximation space, $V_{L;J} = span\{\mu_{ji}\}_{j<J}$. The quadrature rule is based on the use of filters $D_{L;m}^J = < S_{L;J,m}, \theta_{J-1,0} >$ which are well localized and hence can be truncated for a given accuracy [30]. This finite filter length leads to an $O(N)$ algorithm where N denotes the number of degrees of freedom, *i.e.* the number of light-grey wavelet coefficients in Fig. 6. Let us furthermore mention that the method works for arbitrary index sets, *i.e.* no tree structure of the wavelet coefficients is required.

The algorithms for the vaguelette decomposition, sketched above, and for the adaptive wavelet reconstruction, which is analogous, can be found in [30].

10.1.5   Summary of the algorithm

The essential ingredients of the above algorithm can be summarized as follows:

- The use of orthogonal wavelets and of operator adapted vaguelettes diagonalizes the stiffness matrix and avoids assembling and solving of a linear system.

- The cardinal function allows an easy projection and a decomposition compatible with the operator.

- The localization properties of wavelets lead to a fast decay of the functions, and the associated filters which therefore can be truncated up to a given precision.

- The hierarchical organisation of the basis enables the construction of fast pyramidal algorithms, with $O(N)$ complexity.

10.2   Adaptive wavelet scheme for the 2D Navier–Stokes equations

Using a two-dimensional Multi-Resolution Analysis (MRA) obtained through tensor product of two one–dimensional MRA's the above algorithm can be extended to two dimensions. The solution is then developed into a two–dimensional wavelet series $u(x,y) = \sum_j \sum_{i_x,i_y} \sum_{\kappa=1}^3 \tilde{u}_{j,i_x,i_y}^\kappa \psi_{j,i_x,i_y}^\kappa (x,y)$.

Due to the fact that the operator L is not separable, *i.e.* $L \neq L_x L_y$, *e.g.* for $L = Id - \partial_{xx} - \partial_{yy}$ the same holds for the operator adapted biorthogonal functions: $\theta(x,y) = L^{\star-1}\psi(x,y) \neq \theta(x)\theta(y)$ and $\mu(x,y) = L\psi(x,y) \neq \mu(x)\mu(y)$ and similarly for the filters S_L and D_L.

Now we extend the previouly described adaptive wavelet-vaguelette algorithm to solve the two–dimensional Navier–Stokes equations written in

vorticity-velocity formulation. Using this method the vorticity is decomposed into a lacunary basis of orthogonal wavelets. Adaptivity means that the simulation uses only the minimum number of wavelet modes necessary to represent the vorticity field at any given time and position (within a given precision ϵ). We will now use the reduced set of wavelet basis functions to directly compute the evolution of the flow using the discretization procedure described in the previous section.

We expand the vorticity ω into an orthogonal wavelet series (7.1) and apply a Petrov–Galerkin scheme with test functions

$$\theta^\kappa_{j,i_x,i_y}(x,y) = (\gamma - \nu\nabla^2)^{-1}\,\psi^\kappa_{j,i_x,i_y}(x,y) \qquad (10.10)$$

where $\gamma = 3/(2\Delta t)$ The vaguelettes θ defined in (10.10) can be calculated explicitly in Fourier space and have localization properties similar to those of wavelets [42], [27], i.e. in the case of spline wavelets they have exponential decay. The solution then reduces to the calculation of the coefficients

$$
\begin{aligned}
\tilde{\omega}^{\kappa,n+1}_{j,i_x,i_y} &= \; <\omega^{n+1}, \psi^\kappa_{j,i_x,i_y}> \qquad\qquad\qquad\qquad (10.11)\\
&= \; <\frac{4}{3}\gamma\omega^n - \frac{1}{3}\gamma\omega^{n-1}, \theta^\kappa_{j,i_x,i_y}> - <\vec{v}^*\cdot\nabla\omega^*, \theta^\kappa_{j,i_x,i_y}>
\end{aligned}
$$

with $\vec{v}^* = 2\vec{v}^n - \vec{v}^{n-1}$ and $\omega^* = 2\omega^n - \omega^{n-1}$, using an adaptive two-dimensional vaguelette decomposition [4], i.e. only the coefficients $\tilde{\omega}^{\kappa,n+1}_{j,i_x,i_y}$ larger than the threshold ϵ are calculated. The pyramidal decomposition algorithm is based on a subtraction strategy applied to hierarchical nested grids using the cardinal Lagrange function of the operator-adapted multiresolution analysis [27]. Subsequently, the vorticity field is reconstructed on a locally refined grid using the adaptive wavelet reconstruction.

The nonlinear term $\vec{v}^\star\cdot\nabla\omega^\star$ is computed by partial collocation [52]. This pseudo–wavelet scheme can be sketched as follows: starting from the wavelet coefficients of ω^n, ω^{n-1} we obtain the values of $\omega^\star$ on a locally refined grid through an inverse wavelet transform. Solving the Poisson equation using a Petrov–Galerkin scheme with test functions $(\nabla^2)^{-1}\,\psi^\kappa_{j,i_x,i_y}(x,y)$, we get the wavelet coefficients of the stream function $\Psi^\star$. Note that these test functions are rapidly decaying in physical space due to the vanishing moments of the wavelets. Applying an inverse adaptive wavelet transform, the stream function is reconstructed on a locally refined grid. Then the velocity $\vec{v}^\star$, the vorticity gradient $\nabla\omega^\star$ and the nonlinear term $\vec{v}^\star\cdot\nabla\omega^\star$ are calculated using finite differences of 4th order on the adaptive grid. Finally, the right hand side of (10.11) is summed up in physical space using the adaptive grid and then the wavelet coefficients of the vorticity ω^{n+1} are calculated using the adaptive vaguelette decomposition [27].

If the smoothness of ω varies strongly in space and time, it is appropriate to use an adaptive spatial discretization that is re-calculated at each time-step. Adaptivity is also important in order to follow the strong gradients

produced by the coherent vortices as the move around. For the wavelet discretization used here the tracking procedure is accomplished by restricting the full index set

$$\Lambda_J = \{(j, i_x, i_y, \kappa) | (j \quad = \quad 0, \ldots, J-1), (i_x = 0, \ldots, 2^j - 1), (i_y = 0, 2^j - 1),$$
$$(\kappa = 1, 2, 3)\} \qquad\qquad (10.12)$$

to some subset $\Lambda_\epsilon^n \subset \Lambda_J$ which depends on the required tolerance ϵ. The elements designated by Λ_ϵ^n are termed the 'lacunary basis' and correspond to the 'compressed' wavelet coefficients $|\tilde{\omega}_{j,i_x,i_y}^{\kappa,n}| > \epsilon$. The orthogonality of the basis and the decay of the wavelet coefficients relate this to the L^2- approximation error, which can therefore be evaluated.

The adaptivity algorithm then operates as follows: from the previous time-step one determines those indices with coefficients larger than the threshold ϵ. One prepares a 'security zone', to allow for the evolution of the solution in time by adding to each index of this set its neighbouring indices in wavelet space. The solution is then advanced in time by performing a reconstruction of the solution $\omega^\star$ onto the locally refined grid (this minimizes energy loss due to re-gridding). The r.h.s. is then evaluated at these points. Finally, the decomposition onto the operator-adapted basis is applied to determine the new wavelet amplitudes $\tilde{\omega}^{n+1}$. Thus the adaptive algorithm calculates only those wavelet modes that are active (plus a security zone), while the inverse transform ensures that the energy of the neglected modes is re-injected back onto the locally refined grid. Recall that in the inverse transform all wavelet coefficients which have been calculated are evaluated, so that no coefficients are set to zero. The reduction of the index set is only performed afterwards. Finally, let us mention that the complexity of the algorithm is of $O(N_c)$, where N_c denotes the number of wavelet coefficients which are calculated.

Remark:
In the case of two-dimensional turbulence the complexity of a DNS increases like $Re = CN$ (with $C = 1$ for Fourier and $C = 3$ to 7 for grid point methods, depending on the order of the scheme employed). The pseudo-spectral methods have a computational cost of $O(N \log_2 N)$, while the adaptive wavelet method has a computational cost of only $O(N_c)$.

10.3   Application to a 2D turbulent mixing layer

10.3.1   Adaptive wavelet computation

In [21, 55] we studied a temporally developing mixing layer, cf. Fig. 8. The initial velocity has a hyperbolic–tangent profile $u(y) = U \tanh(2y/\delta_0)$ which implies a vorticity thickness $\delta_0 = 2U/(du/dy)|_{y=0}$. From linear stability analysis the mixing layer is known to be inviscidly unstable. A perturbation

leads to the formation of vortices by Kelvin–Helmholtz instability, where
the most amplified mode corresponds to a longitudinal wavelength $\lambda = 7\delta_0$.
The initial vorticity thickness δ_0 is chosen such that 10 vortices should
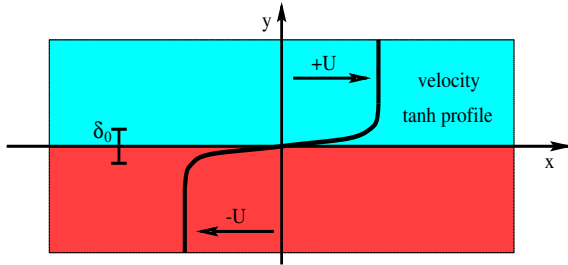
Fig. 8. Initial configuration for the mixing layer.

develop in the numerical domain of size $[0, 2\pi]^2$. To trigger the instability
we superimposed a weak white noise in the rotational region. The velocity
is $U \approx 0.1035$ and the viscosity is $\nu = 5 \cdot 10^{-5}$. For the numerical simulation
we employ a maximal resolution of 256×256, which corresponds to $L = 8$,
and cubic spline wavelets of Battle–Lemarié type. The time step is $\Delta t =
2.5 \cdot 10^{-3}$. The threshold for the wavelet coefficients was $\epsilon_0 = 10^{-6}$ and
10^{-5}.

In Fig. 9 (left) we compare the energy spectrum at $t = 37.5$ of a DNS
computation using a classical pseudo-spectral method, with two wavelet
computations using different thresholds ($\epsilon_0 = 10^{-6}$ and 10^{-5}).
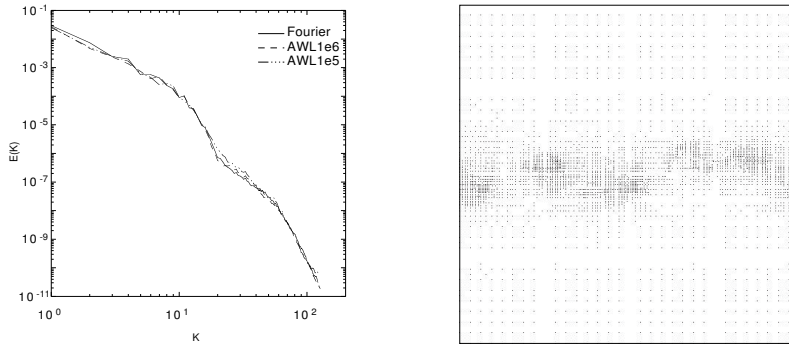

Fig. 9. Left: energy spectra for the pseudo-spectral reference run and for the
adaptive wavelet simulations with thresholds $\epsilon_0 = 10^{-6}, 10^{-5}$. Right: adaptive
grid reconstructed from the index set of the retained wavelet coefficients. Both at
time $t = 37.5$.

Fig. 9 (left) shows that all scales of the flow are well-resolved for both
thresholds. The underlying grid Fig. 9 (right) which corresponds to the
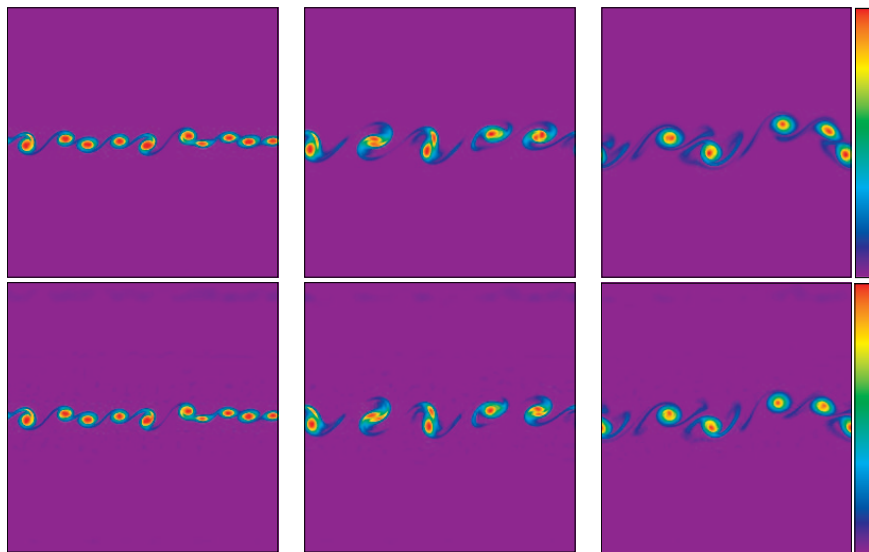
Fig. 10. ω at $t = 12.5,\ 25,\ 37.5$. Top: pseudo-spectral method. Bottom: adaptive wavelet method ($\epsilon_0 = 10^{-6}$).
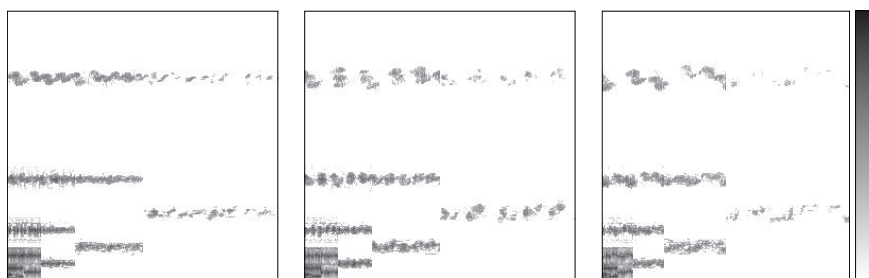

Fig. 11. Active wavelet coefficients at $t = 12.5,\ 25,\ 37.5$. ($\epsilon_0 = 10^{-6}$).

centers of active wavelets for the computation with $\epsilon_0 = 10^{-6}$ at $t = 37.5$ shows a local refinement in regions of strong gradients.

10.3.2   Comparison between CVS and Fourier pseudo-spectral DNS

In Fig. 10 (bottom) we show the evolution of the vorticity field for the adaptive wavelet simulation with threshold $\epsilon_0 = 10^{-6}$ and for the reference pseudo–spectral computation (top). In both simulations, as predicted by the linear theory, 10 vortices are formed, which subsequently undergo successive mergings. In Fig. 11 the active wavelet coefficients (gray entries) are plotted using a logarithmic scale. The coefficients $\tilde{\omega}_\lambda$ are placed at position $(x_1, x_2) = (2^j(1-\delta_{d,1}) + k_x,\ 2^j(1-\delta_{d,2}) + k_y)$ with the origin in the lower left
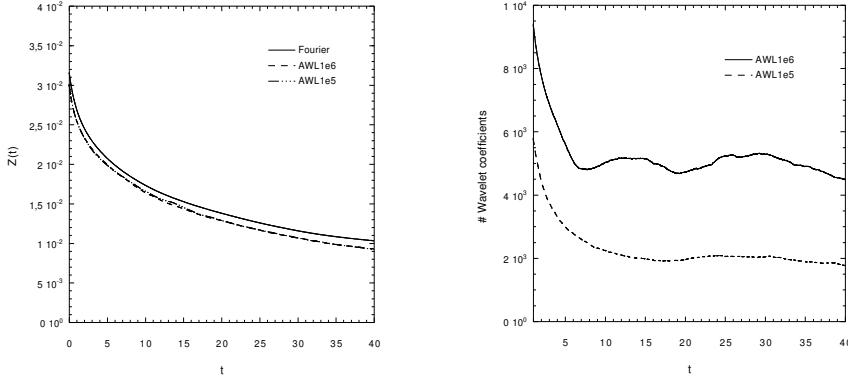
Fig. 12. Left: evolution of enstrophy. Right: evolution of #DOF. ($\epsilon_0 = 10^{-6}, 10^{-5}$).

corner and the y-coordinate oriented upwards, from coarser to finer scales. We observe that the basis dynamically adapts to the flow evolution during the computation with only 8% of the coefficients being used. We observe that in the wavelet simulation the formation and evolution of vortices are well captured, although we find that at later times a slight phase shift appears with respect to the DNS (top). This might be due to the fact that the retained wavelet coefficients contain 94% of the total enstrophy, as observed in Fig. 12 (left) which shows the time evolution of the total enstrophy using the different thresholds. The 6% loss of enstrophy comes from the fact that in the wavelet simulations we have not modelled the effect of the discarded modes onto the retained ones. This will be considered in future work, where the enstrophy of the discarded wavelets will be reinjected into the coherent vortices using the wavelet forcing method we have proposed [50].

Finally, we plot the time evolution of the number of degrees of freedom for the two wavelet runs in Fig. 12 (right). First, we observe an initial phase, up to $t = 7$ s, where there is a strong reduction in the number of active modes, which corresponds to the formation of the coherent vortices. Then the number of active modes remains almost constant, and represent a significant reduction of the number of modes, with $N_{ad} = 5000$ for $\epsilon_0 = 10^{-6}$ and $N_{ad} = 2000$ for $\epsilon_0 = 10^{-5}$ out of $N = 65536$ initial modes.

Part IV
Conclusion

In these lecture notes we have reviewed wavelet techniques for analyzing and computing turbulent flows. We summarized the continuous and orthogonal wavelet transforms and presented the algorithms for their numerical implementation. Furthermore we presented classical and some recently developed wavelet-based statistical tools for analyzing turbulent flows.

We then described a wavelet-based method designed for computing turbulent flows, called CVS (Coherent Vortex Simulation). The CVS filtering consists of projecting the vorticity field onto an orthogonal wavelet basis and decomposing it into two orthogonal components using a nonlinear thresholding of the wavelet coefficients. The coherent vorticity field is reconstructed from the few wavelet coefficients larger than a given threshold, which depends only on the resolution and on the total enstrophy, while the incoherent vorticity is reconstructed from the many remaining weak wavelet coefficients. The coherent and incoherent velocity fields are then derived from the coherent and incoherent vorticity fields using Biot–Savart's integral equation.

We applied the CVS filtering to a 3D turbulent mixing layer. We have shown that few strong wavelet coefficients represent the coherent vortices, the whole energy spectrum and the whole vorticity PDF. In contrast, many weak wavelet coefficients represent the incoherent background flow, which is structureless, exhibits an energy equipartition spectrum and an exponential distribution for the vorticity PDF. This demonstrates the advantage of the CVS filtering in comparison to the LES filtering, since we have shown that the small scale flow, which is discarded in LES, exhibits many coherent structures, has a much wider PDF of vorticity and does not present an energy equipartition spectrum.

We then presented an adaptive wavelet computation of a 2D mixing layer and shown the dynamical adaption of the grid in physical space which allows to follow the flow evolution with a reduced number of active degrees of freedom. We showed that the adaptive wavelet method produces accurate results with fewer active modes than the classical pseudo-spectral method. The classical pseudo–spectral method does not exploit the vortical structure of high Reynolds number flows, while the adaptive wavelet method does, which leads to greater efficiency at high Reynolds numbers.

In conclusion, although the numerical method we propose is Eulerian, based on a Galerkin scheme, its adaptive character, in both space and scale, allows to track the displacements and deformations of active flow regions, as Lagrangian methods would do.

References

[1] W.T. Ashurst, A.R. Kerstein, R.M. Kerr and C.H. Gibson, *Phys. Fluids* **30**(8), 2343 (1987).

[2] G.K. Batchelor. *Homogeneous turbulence*, Cambridge University Press (1953).

[3] G. Beylkin, R. Coifman, and V. Rokhlin. Fast wavelet transforms and numerical algorithms I. *Comm. Pure Appl. Math.*, **44**, 141 (1991).

[4] H. Bockhorn, J. Fröhlich and K. Schneider. An adaptive two–dimensional Wavelet–Vaguelette Algorithm for the Computation of Flame balls . *Combust. Theory Modelling*, **3**, 177–198 (1999).

[5] C. Canuto, M.Y. Hussaini, A. Quaternioni and T.A. Zang, *Spectral Methods in Fluid Dynamics* (Springer-Verlag, Berlin, 1988).

[6] P. Charton and V. Perrier. A pseudo–wavelet scheme for the two–dimensional Navier–Stokes equation. *Comp. Appl. Math.*, **15**, 139–160 (1996).

[7] Chorin, A. J. (1994). *Vorticity and turbulence*, (Springer).

[8] I. Daubechies, *Ten Lectures on Wavelets* (SIAM, Philadelphia, 1992).

[9] P. E. Dimotakis and H. J. Catrakis, Turbulence, fractals and mixing. *Mixing, chaos and Turbulence*, Eds. H. Chaté, E. Villermaux and J.M. Chomaz, NATO ASI Series, Serie B: Physics **373**, 59–144, Kluwer (1999).

[10] M. Do–Khac, C. Basdevant, V. Perrier and K. Dang–Tran. Wavelet analysis of 2d turbulent flows. *Physica D*, **76**, 252–277 (1994).

[11] D. Donoho. Wavelet shrinkage and Wavelet -Vaguelette Decomposition: a 10–minute tour, *in* "Progress in Wavelet Analysis and Applications", pp. 109–128, Proc. Int. Conf. "Wavelets and Applications", Toulouse, June 1992.

[12] D. Donoho, I. Johnstone, G. Kerkyacharian, D. Picard. Wavelet shrinkage: Asymptopia? (with discussion) *J. Royal Stat. Soc., Ser. B* **57**, 301–369 (1995).

[13] D.G. Dritschel and D.W. Waugh, *Phys. Fluids* A **4**(8), 1737 (1992).

[14] M. Farge, Wavelet Transforms and their Applications to Turbulence, *Ann. Rev. of Fluid Mech.*, **24**, 395–457 (1992).

[15] M. Farge, J.-F. Colonna and M. Holschneider, in *Topological Fluid Mechanics*. Eds. H.K. Moffatt and A. Tsinober (Cambridge University Press), 765–776 (1989).

[16] M. Farge, E. Goirand, Y. Meyer, F. Pascal, M.V. Wickerhauser, Improved predictability of two-dimensional turbulent flows using wavelet packet compression, *Fluid Dynamics Research*, *10*, 229–250 (1992).

[17] M. Farge and G. Rabreau. Transformée en ondelettes pour detecter et analyser les structures coherents dans les ecoulements turbulents bidimensionnels, *C. R. Acad. Sci. Paris Série II* **307**, 1479 (1988).

[18] M. Farge, Y. Guezennec, C.M. Ho, C. Meneveau. Continuous wavelet analysis of coherent structures, *Proceedings of the 1990 Summer Program, Center for Turbulence Research*, NASA-Ames and Stanford University, 331-348, (1990).

[19] M. Farge, K. Schneider and N. Kevlahan. Coherent structure eduction in wavelet–forced two–dimensional turbulent flows. *IUTAM Symposium on Dynamics of slender vortices (Eds. E. Krause and K. Gersten)*, Kluwer Academic Publishers, 65–83 (1998).

[20] M. Farge, N. Kevlahan, V. Perrier and K. Schneider. Turbulence analysis, modelling and computing using wavelets. *Wavelets in Physics* (Ed. J.C. van den Berg), Cambridge University Press, 117–200 (1999).

[21] M. Farge, K. Schneider and N. Kevlahan. Non–Gaussianity and Coherent Vortex Simulation for two–dimensional turbulence using an adaptive orthonormal wavelet basis. *Phys. Fluids*, **11** (8), 2187–2201 (1999).

[22] M. Farge and K. Schneider. Coherent Vortex Simulation (CVS), a semi-deterministic turbulence model using wavelets. *Flow, Turb. Combust.*, submitted.

[23] M. Farge, G. Pellegrino and K. Schneider. Coherent vortex extraction in 3D turbulent flows using orthogonal wavelets. Preprint, 2000, *Phys. Rev. Lett.*, submitted.

[24] J. H. Ferziger. Large Eddy Simulation. *Simulation and Modeling of Turbulent Flows.* (Eds. T. B. Gatski, M. Y. Hussaini and J. L. Lumley), ICASE Series in Computational Science and Engineering, 109 (1992).

[25] U. Frisch. *Turbulence. The legacy of A.N. Kolmogorov.* Cambridge University Press (1995).

[26] J. Fröhlich and K. Schneider. An adaptive wavelet Galerkin algorithm for one– and two–dimensional flame computation, *Eur. J. Mech.* B, **13**, 439–471 (1994).

[27] J. Fröhlich and K. Schneider. A fast algorithm for lacunary wavelet bases related to the solution of PDE's. *C. R. Math. Rep. Acad. Sci. Canada* **17**(6), 283 (1995).

[28] J. Fröhlich and K. Schneider. Numerical simulation of decaying turbulence in an adaptive wavelet basis. *Appl. Comput. Harm. Anal.* **3**, 393–397 (1996).

[29] J. Fröhlich and K. Schneider. Computation of Decaying Turbulence in an Adaptive Wavelet Basis. *Physica D*, **134** 337–361 (1999).

[30] J. Fröhlich and K. Schneider An Adaptive Wavelet–Vaguelette Algorithm for the Solution of PDE's, *J. Comput. Phys.*, **130**, 174–190 (1997).

[31] A. Grossmann and J. Morlet. Decomposition of Hardy functions into square integrable wavelets of constant shape. *SIAM J. Math. Anal.*, **15**, 723–736 (1984).

[32] M. Germano, U. Piomelli, P. Moin and W. H. Cabot. A dynamic subgrid scale model eddy viscosity model. In *Proceedings Summer Workshop, Center for Turbulence Research, Stanford* (1990).

[33] M. Holschneider and Ph. Tchamitchiam. *Regularité locale de la fonction non-differentiable de Riemann*, in *Les ondelettes en 1989*, Lecture Notes in Mathematics, P.G. Lemarié (Ed.), Springer (1989).

[34] N. K.-R. Kevlahan and M. Farge. Vorticity filaments in two–dimensional turbulence: creation, stability and effect. *J. Fluid Mech.*, *346*, 49–76 (1997).

[35] A.N. Kolmogorov, The Local Structure of Turbulence in Incompressible Viscous Fluid for Very Large Reynolds Numbers. *C. R. Acad. Sc. USSR*, **30**, 301–305 (1941).

[36] R. Kraichnan. Inertial ranges in two–dimensional turbulence. *Phys. Fluids*, **10**, 1417–1423 (1967).

[37] A. Leonard. Energy cascade in Large Eddy Simulations of turbulent fluid flows. *Adv. Geophys.* **18 A**, 237 (1974).

[38] J. Liandrat and Ph. Tchamitchian, *Resolution of the 1D Regularized Burgers Equation Using a Spatial Wavelet Approximation Algorithm and Numerical Results*, (ICASE, 1990).

[39] S. Mallat. *A wavelet tour to signal processing.* Academic Press (1997).

[40] C. Meneveau. Analysis of turbulence in the orthonormal wavelet representation. *J. Fluid Mech.*, **232**, 469–520 (1991).

[41] M.V. Melander, N.J. Zabusky and J.C. McWilliams, *J. Fluid Mech.* **195**, 303 (1988).

[42] Y. Meyer, *Ondelettes et Opérateurs I/II* (Hermann, Paris, 1990).

[43] A.S. Monin and A.M. Yaglom. *Statistical Fluid Mechanics: Mechanics of Turbulence*, (The M.I.T. Press 1975).

[44] R. Murenzi. Wavelet transforms associated to the n–dimensional Euclidean Group with dilatations. PhD thesis, UCL, Louvain-la-Neuve (1989).

[45] J. von Neumann, 1949. Recent theories of turbulence, in *Collected works (1949–1963)* **6**, Ed. A. H. Taub. (Pergamon Press, 1963), p. 437.

[46] V. Perrier and C. Basdevant. La décomposition en ondelettes périodiques, un outil pour l'analyse de champs inhomogènes. Théorie et algorithmes. *Rech. Aérosp.*, **3**, 53 (1989).

[47] V. Perrier, T. Philipovich and C. Basdevant. Wavelet spectra compared to Fourier spectra. *J. Math. Phys.*, **36**(3), 1506–1519 (1995).

[48] M. Rogers and R. Moser. Direct simulation of a self-similar turbulent mixing layer. *Phys. Fluids*, **6**(2), 903–923 (1994).

[49] P.G. Saffman. *Vortex Dynamics*. (Cambridge University Press 1972).

[50] K. Schneider and M. Farge. Wavelet forcing for numerical simulation of two–dimensional turbulence. *C. R. Acad. Sci. Paris Série II* **325**, 263–270 (1997).

[51] K. Schneider, N. Kevlahan and M. Farge. Comparison of an adaptive wavelet method and nonlinearly filtered pseudo-spectral methods for two-dimensional turbulence. *Theoret. Comput. Fluid Dynamics*, **9** (3/4), 191–206 (1997).

[52] K. Schneider, N. Kevlahan and M. Farge. An adaptive wavelet method compared to nonlinearly filtered pseudo-spectral methods for two-dimensional turbulence. *Advances in Turbulence VII (Ed. U. Frisch)*, Kluwer Academic Publishers, 147–150 (1998).

[53] K. Schneider and M. Farge. Wavelet approach for modelling and computing turbulence. *Lecture Series 1998–05 Advances in turbulence modelling*, von Karman Institute for Fluid Dynamics, Bruxelles, 132 pages (1998).

[54] K. Schneider, M. Farge and N. Kevlahan. Intermittency and coherent vortices in fully–developed two–dimensional turbulence. Preprint, ICT Universität Karlsruhe (1999).

[55] K. Schneider and M. Farge. Numerical simulation of a mixing layer in an adaptive wavelet basis. *C. R. Acad. Sci. Paris Série II b*, 263–269 (2000).

[56] R. Teman. *Navier–Stokes equations and nonlinear functional analysis*. SIAM, Philadelphia (1983).

[57] A. Vincent, iand M. Meneguzzi. The spatial structure and statistical properties of homogeneous turbulence. *J. Fluid Mech.*, **225**, 1–20 (1991).

[58] A. Vincent and M. Meneguzzi. *J. Fluid Mech.* **258**, 245 (1994).